PROF. PIERRE MORSOMME (Orcid ID : 0000-0001-7780-7230)

PROF. FRANÇOIS CHAUMONT (Orcid ID : 0000-0003-0155-7778)

Article type : Regular Manuscript

Title:

Plasma membrane aquaporins interact with the endoplasmic reticulum resident VAP27 proteins at ER-PM contact sites and endocytic structures

Authors: Ana Romina Fox[1,2], Florencia Scochera[2,3], Timothée Laloux[1], Karolina Filik[1], Hervé Degand[1], Pierre Morsomme[1], Karina Alleva[2,3] and François Chaumont[1]

Affiliations:

[1]Louvain Institute of Biomolecular Science and Technology, UCLouvain, 1348 Louvain-la-Neuve, Belgium.

[2]Universidad de Buenos Aires, CONICET, Facultad de Farmacia y Bioquímica, Instituto de Química y Fisicoquímica Biológica (IQUIFIB), 1113 Buenos Aires, Argentina.

[3]Universidad de Buenos Aires, Facultad de Farmacia y Bioquímica, Departamento de Fisicomatemática, 1113 Buenos Aires, Argentina.

ORCID

Ana Romina Fox, https://orcid.org/0000-0002-7852-4539

Karolina Filik, https://orcid.org/0000-0002-8086-038X

Pierre Morsomme, https://orcid.org/0000-0001-7780-7230

Karina Alleva, https://orcid.org/0000-0002-9081-2103

François Chaumont, https://orcid.org/0000-0003-0155-7778

Author for correspondence:

François Chaumont

Tel: +32 10 47 84 85

Email address: francois.chaumont@uclouvain.be

Received: *3 April 2020*

Accepted: *1 June 2020*

Summary

- Plasma membrane (PM) intrinsic proteins (PIPs) are aquaporins facilitating the diffusion of water and small solutes. The functional importance of the PM organization of PIPs in the interaction with other cellular structures is not completely understood.
- We performed a pull-down assay using maize (*Zea mays*) suspension cells expressing YFP-*Zm*PIP2;5 and validated the protein interactions by yeast split-ubiquitin and bimolecular fluorescence complementation assays. We expressed interacting proteins tagged with fluorescent proteins in *Nicotiana benthamiana* leaves and performed water transport assays in oocytes. Finally, a phylogenetic analysis was conducted.
- The PM located *Zm*PIP2;5 physically interacts with the endoplasmic reticulum (ER) resident *Zm*VAP27-1. This interaction requires the *Zm*VAP27-1 cytoplasmic major sperm domain. *Zm*PIP2;5 and *Zm*VAP27-1 localize in close vicinity in ER/PM contact sites (EPCSs) and endocytic structures upon exposure to salt stress conditions. This interaction enhances PM water

permeability in oocytes. Similarly, the Arabidopsis *Zm*VAP27-1 paralog, *At*VAP27-1, interacts with the *At*PIP2;7 aquaporin.

- Together, these data indicate that the PIP2-VAP27 interaction in EPCSs is evolutionarily conserved, and suggest that VAP27 might stabilize the aquaporins and guide their endocytosis in response to salt stress.

Key words: aquaporin, endocytosis, endoplasmic reticulum (ER), endoplasmic reticulum/plasma membrane (ER/PM) contact sites (EPCSs), plasma membrane intrinsic protein (PIP), plant vesicle-associated membrane protein (VAMP)-associated protein (VAP27).

Introduction

Plasma membrane (PM) intrinsic proteins (PIPs) are aquaporins that facilitate the diffusion of water and small solutes through lipid bilayers (Maurel *et al.*, 2015; Fox *et al.*, 2017). PIP main function is exerted at the PM, where different lateral channel diffusion patterns exist (Li *et al.*, 2011). Some channels move freely, whereas others localize in restricted lateral diffusion regions such as microdomains (Li *et al.*, 2011). Interestingly, other cellular structures besides the PM, such as the cell wall (Martiniere *et al.*, 2012) and actin filaments (Hosy *et al.*, 2015), are involved in PIP lateral diffusion restriction, which reflects PIP close interaction with other cellular structures. The functional importance of PIP PM organization in interactions with proteins/lipids from other cellular structures is not completely understood, but the role of PIP microdomains in the regulation of exo/endocytosis was proposed (Takano *et al.*, 2017).

Inter-organelle contacts through membrane contact sites are involved in the maintenance of phospholipid homeostasis and trafficking events (Pérez-Sancho *et al.*, 2016). These contact types among organelles are not randomly established but follow patterns that change when cellular nutrient status is modified or the cytoskeleton disassembled (Valm *et al.*, 2017). Recently, it was shown that ER-PM contact sites (EPCSs) were enhanced by ionic stress (Lee *et al.*, 2019), which is especially relevant for plant cells. EPCS proteomes are not yet clearly established, but evidence points to the existence of different EPCS populations (Siao *et al.*, 2016; Stefano *et al.*, 2018). In

recent years, plant vesicle-associated membrane protein (VAMP)-associated proteins (VAP27s) and synaptotagmins (SYTs) have been characterized as evolutionarily conserved ER tethers that maintain the ER membrane in close proximity to the PM without fusing them (Wang *et al.*, 2014; Pérez-Sancho *et al.*, 2015; Wang *et al.*, 2016). Arabidopsis STY1 interacts with the SNARE SYP121 and is involved in endocytosis and endosome recycling to the PM (Lewis & Lazarowitz, 2010; Kim *et al.*, 2016). Also, plant VAP interaction with a specific phosphoinositides (PI) subset in clathrin-mediated endocytosis has been reported (Stefano *et al.*, 2018). Consistently, in ER-endosome membrane contact sites from mammal cells, VAPs are necessary to downregulate specific PI endosome levels and to ensure correct actin filament deposition (Dong *et al.*, 2016). Remarkably, PIP endocytosis and autophagic degradation occurs in a PI-dependent manner (Ueda *et al.*, 2016; Jurkiewicz *et al.*, 2020), and different PIP isoforms are highly expressed in cell elongation zones (Heinen *et al.*, 2009), regions where the EPCSs are abundant (McFarlane *et al.*, 2017). However, evidence for PIPs presence at EPCSs has not been shown yet.

Complex post-translational regulation of eukaryotic aquaporins is mediated by other proteins (Roche & Törnroth-Horsefield, 2017). For instance, hundreds of putative *At*PIP interactors were found (Bellati *et al.*, 2016). PIP cytosolic domains (i.e. the N- and C-termini, loop B and D) are involved in regulation of channel trafficking, degradation, and gating upon interaction with specific proteins (Lee *et al.*, 2009; Zelazny *et al.*, 2009; Wu *et al.*, 2013; Hachez *et al.*, 2014a; Grondin *et al.*, 2015; Li *et al.*, 2015; Afzal *et al.*, 2016; Bellati *et al.*, 2016). In the present work, we explore which are the main partners of maize (*Zea mays*) *Zm*PIP2;5, the most highly expressed PIP isoform in roots involved in radial water movement (Hachez *et al.*, 2006; Ding *et al.*, 2020). We found that *Zm*PIP2;5 interacts with VAP27s inserted in the ER membrane, and that this interaction positively influences PM water permeability. We propose that VAP27s stabilize PIP2s at the PM and might guide their endocytosis in response to salt stress. This interaction seems to be conserved through land plant evolution.

Material and Methods

Genetic constructs

Total RNA was extracted from 6-d-old maize Black Mexican Sweet (BMS) cells using the RNeasy Plant Mini Kit (Qiagen, Hilden, Germany) following the manufacturer's instructions.

Total cDNA was synthesized from RNA (1 µg) in a 25 µl reaction using the M-MLV Reverse Transcriptase (Promega, Madison, USA) and the OligodT(15) primer. For the SUS assay, *Zm*VAP27-1 and *Zm*VAP27-2 cDNAs were PCR amplified from BMS cell total cDNA, and *ZmPIP2;5* cDNA, optimized for expression in yeast, was PCR amplified from pYeDP60u-*Zm*PIP2;5^{OPT} (Bienert *et al.*, 2014) using the corresponding att1B and att2B primers (Table S1). The PCR products were cloned with the Gateway® system (Invitrogen, Waltham, USA) into the pDONR221P1P2 entry vector prior to their integration in the SUS destination vectors. The pMetYC-DEST and pNX35-DEST (Grefen *et al.*, 2009) were used to produce the Met-repressible bait construct *ZmPIP2;5-Cub-PLV* and the prey constructs *NubG-ZmVAP27-1* or *NubG-ZmVAP27-2*, respectively. The NubWT control fragment was obtained from the pNubWT-Xgate vector (Grefen *et al.*, 2009).

To carry out bimolecular fluorescence complementation (BiFC) and localization assays the cDNAs were cloned with the Gateway® system (Invitrogen). Briefly, *ZmPIP2;5* and *ZmVAP27-1* were PCR amplified using the corresponding attB1 and attB4 primers and cloned into the pDONR221P1P4 entry vector. *ZmSYP121*, *ZmVAP27-1*, *ZmVAP27-2*, *AtVAP27-1*, *NpPMA2* and the deleted *ZmVAP27-1* versions (ΔMSD and ΔTMD) were PCR amplified using the corresponding attB3 and attB2 primers. For the ΔCCD mutant genetic construct, two PCR fragments obtained with the attB3AtVAP27-1NFw/RvVAP11deltaCCD and attB2AtVAP27-1NRv/FwVAP11deltaCCD primer pairs were assembled in a second PCR with the attB3 and attB2 primers. All these PCR fragments were cloned into the pDONR221P3P2 entry vector. The plasmid *pDONR221P1P4-AtPIP2;7* was previously published by our lab (Hachez *et al.*, 2014a). The vector Gateway® cassettes were transferred to the pBIFCt-2in1-NN destination vector (Grefen & Blatt, 2012) and/or the pFRETtv-2in1-NN (Hecker *et al.*, 2015).

For the oocyte swelling assays, the pT7Ts-derived vector containing the T7 RNA polymerase promoter and carrying the 5' and 3' translated regions of the *Xenopus laevis* β globin gene (Gorgoni *et al.*, 1995) was modified to add new cloning sites. Briefly, overlapping oligos with the recognition sites for *Not*I, *Xho*I, and *Sac*II (Table S1) were annealed and cloned in the vector previously linearized using the *Bgl*II and *Spe*I enzymes. The *ZmPIP2;5* and *ZmVAP27-1* cDNAs were PCR amplified from BiFC vectors using specific primers to add restriction enzyme sites (Table S1). *ZmPIP2;5* was cloned into the *Bgl*II and *Spe*I sites, and *Zm*VAP27-1 was cloned into the *Sac*II and *Spe*I sites. All cloned products were checked by sequencing.

Transfection of maize BMS cells

BMS cells were cultivated in the dark with constant shaking at 90 rpm and 25°C, in BMS medium (50 ml) (4.4 g l^{-1} Murashige and Skoog basal salts with minimal organics (M6899, Sigma Aldrich, St. Louis, USA), 30 g l^{-1} Sucrose, 3 mg l^{-1} 2,4-dichloro-phenoxyacetic acid (D8407, Sigma Aldrich), and 0.2 g l^{-1} of L-Asn (A4284, Sigma Aldrich), pH 5.8). The cells were subcultured every 14 days at a 1:10 ratio with fresh BMS medium at room temperature.

Stable transfected BMS cells were obtained using the PDS-1000/He Biolistic particle bombardment delivery system (BioRad, Hercules, USA). Briefly, *pCAMBIA35Su:YFP-PIP2;5* (Chevalier *et al.*, 2014) and *pCAMBIA35Su:YFP* (Ding *et al.*, 2020) DNAs were precipitated onto 0.6 µm gold particles. These DNA-coated particles were used to bombard 9-d-old BMS cells spread over Whatman filters on top of BMS medium-agar plates. After 3 days the filters were transferred to selective BMS-medium plates (Kanamycin 100 µg ml^{-1} for *pCAMBIA35Su:YFP-PIP2;5* and Bialaphos 3 µg ml^{-1} for *pCAMBIA35Su:YFP*). Every 15 days the filters were transferred to fresh plates. Fluorescent calli were selected after 4-6 weeks.

Protoplast swelling assay

BMS protoplast isolation was performed as described previously (Moshelion *et al.*, 2004). Briefly, protoplasts were isolated from 2 ml of 8-d-old BMS cell suspensions. The cells were left to sediment and the BMS medium was replaced with cell wall digestion solution (1 ml) (1.5% w/v cellulase Y-C (Kyowa Chemical products, Japan), 0.3% w/v Macerozyme R-10 (Duchefa Biochemie, Haarlem, The Netherlands) in isotonic solution (see below)). The cells were placed on a rotary shaker (90 rpm) for 2 h 30 min at 26°C. Then, the cells were passed through a nylon filter (20 µm pore size) and washed two times with isotonic solution. The protoplast swelling experiments were performed as described previously (Moshelion *et al.*, 2004). The isotonic and hypotonic solutions (10 mM KCl, 1 mM $CaCl_2$, 8 mM MES, pH 5.75) were adjusted with sorbitol to 300-330 and 150-160 mOsm, respectively. The Advanced Instruments 3300 Micro-Osmometer (Advanced Instruments, Massachusetts, USA) served for all osmolarity measurements.

Plant microsomal fraction preparation, immunoprecipitation, and LC-MS assays.

BMS cells were grown in 200 ml cultures and harvested after 7 days. The cells were washed with ice-cold homogenization buffer (250 mM sorbitol, 50 mM Tris-HCl pH 8, 2 mM 2-[2-[bis(carboxymethyl)amino]ethyl-(carboxymethyl)amino]acetic acid (EDTA), 10 mM dithiothreitol (DTT), 1 mM phenylmethylsulphonylfluoride (PMSF), and 2 µg ml^{-1} each of leupeptin, pepstatin, aprotinin, antipain, and chymostatin) and ground with glass beads. Cell debris was removed by centrifugation for 5 min at 3,500 *g*. The supernatant was then centrifuged for 30 min at 100,000 *g*. Finally, the pellet corresponding to the microsomal fraction was suspended in resuspension buffer (250 mM sucrose, 20 mM HEPES pH7.4, 10 mM KCl, 1.5 mM $MgCl_2$, 1 mM EDTA, 1 mM 2-[2-[2-[2-[bis(carboxymethyl)amino]ethoxy]ethoxy]ethyl-(carboxymethyl)amino]acetic acid (EGTA), 10 mM DTT, 1 mM PMSF, and 2 µg ml^{-1} each of leupeptin, pepstatin, aprotinin, antipain, and chymostatin). Proteins were quantified by the Bradford assay (Bradford, 1976) and adjusted to 3 mg ml^{-1} and 1% w/v octyl-β-D-glucopyranoside. Protein extracts (15 mg) were mixed with 30 µl agarose beads (Chromotek, Planegg, Germany) and incubated in a rotor wheel for 1 h at 4°C. Then, the beads were pelleted by centrifugation at 2,000 *g* for 10 s and the supernatant was incubated with 30 µl Chromotek GFP-Trap® agarose beads in a rotor wheel at 4°C overnight (ON). The beads were washed five times with 700 µl resuspension buffer supplemented with 300 mM NaCl. Bound proteins were eluted from the beads by adding 20 µl Laemmli buffer and incubating for 15 min at 65°C. This step was repeated twice. *Zm*PIP2;5 immunoprecipitation was confirmed in aliquots (2 µl) by immunoblot. The remaining samples were electrophoresed by SDS-PAGE just to stack the proteins that were in-gel digested with trypsin, and peptides recovered for the nano-ultra-high performance liquid chromatography coupled with electrospray ionization-quadrupole-time of flight-mass spectrometry (nano-ULPC-ESI-QTOF-MS) analysis at the MASSPROT facility (UCLouvain, detailed protocol in Methods S1). For each sample, three technical replicates were run in the nano-ULPC-ESI-QTOF-MS. Progenesis QI (v.2.0, Nonlinear Dynamics) was used to analyze the spectrometry data. The runs were normalized to YFP levels. For peptide identification the maize UP000007305 reference proteome was used (UniProt). The detailed information of the ions to peptides and peptides to proteins association is in Table S2. Progenesis QI is not prepared to handle technical and biological replicates in the statistical analysis. Therefore, to score the differential abundance of proteins between YFP-*Zm*PIP2;5 and YFP samples including technical replicates, the online freely available RepExplore software

(Glaab & Schneider, 2015) was used. In this software the variance across technical replicates is included in the analysis using a Bayesian approach named probability of positive log ratio (PPLR) statistic (Glaab & Schneider, 2015).

Split-Ubiquitin Assays (SUS)

The haploid yeast strain THY.AP4 was cotransformed by electroporation with the Nub and Cub constructs of interest. Yeast colonies coexpressing the bait and prey constructs were recovered 48 h after transfer to selective media (CSM, -Leu$^-$, Trp$^-$) (Grefen *et al.*, 2009). Growth assays were performed as Hachez *et al.* (2014a). Yeast coexpressing the Met-repressible bait construct *Zm*PIP2;5-Cub-PLV and the prey constructs NubG-*Zm*VAP27-1, NubG-*Zm*VAP27-2, NubG (negative control), or NubWT (positive control) were grown on selective media. The next day, dilution series (OD_{600} nm 0.5, 0.05, and 0.005) of the cultures were dropped onto interaction-selective (CSM, -Leu$^-$, Trp$^-$, Ade$^-$, His$^-$, Met$^-$) medium containing 100 µM methionine to repress bait expression. Control plates without methionine serve to verify that an equal yeast amount had been dropped. Yeast growth was recorded after incubation for 48 h at 30°C. Protein expression was verified via immunoblotting using a rat monoclonal antibody against the hemagglutinin (HA) tag (Roche, Mannheim, Germany) and a rabbit polyclonal antibody against VP16 (Abcam, Cambridge, UK), as previously described (Grefen *et al.*, 2009). Protein loading on PVDF membrane was revealed by Coomassie R250 staining (Goldman *et al.*, 2016).

Confocal microscopy

A Zeiss LSM710 confocal microscope equipped with a spectral detector module (Carl Zeiss, Oberkochen, Germany) was used for confocal image acquisition. Imaging of BMS cells transformed with YFP-*Zm*PIP2;5 was achieved with a C-Apochromat 40x/1.20 water immersion objective. The mYFP molecule was excited with the 514-nm laser lines. Emitted light was collected through a dichroic mirror on detector 520 to 560 nm. The cell PM was stained with FM4-64 dye (16 µM, Invitrogen). This dye was excited at 514 nm and detected from 600 nm to 760 nm.

The BiFC and localization assays were performed in tobacco (*N. benthamiana*) epidermal cells transformed by *Agrobacterium tumefaciens* infiltration (Batoko *et al.*, 2000). Samples were analyzed 3 days after infiltration. For fluorophore excitation and emission, the following laser settings were used: for mRFP1 excitation 561 nm and emission 560 to 615 nm, for mYFP excitation at 514 nm and emission 522 to 553 nm, for mTRQ2 excitation 445 nm and emission 463 to 520 nm, for mVenus excitation 514 nm and emission 520 to 574 nm. The BiFC analysis was performed using a 40×/0.75 water-immersion objective. Images were taken with standardized excitation intensities and photomultiplier gains. Relative fluorescence was analyzed using the ZEN 2 Profile module (blue edition, Carl Zeiss). Five lines of five to six µm length were drawn through the PM of one cell. The fluorescence intensity of each line for each fluorophore was obtained. Then, the mYFP to mRFP1 fluorescence ratio of each line was calculated and averaged for that cell. The neighbor cells were not used to measure the fluorescence intensity to avoid including twice the values of a single cell. When specified the Airyscan module (Carl Zeiss) and Plan-Apochromat ×63/1.40 oil immersion objective were used.

In vitro RNA synthesis and oocyte water transport assays

The capped cRNA encoding for *ZmPIP2;5* was synthesized *in vitro* using the mMESSAGE mMACHINET7 High Yield Capped RNA Transcription Kit (Ambion, Austin, USA), and the capped *ZmVAP27-1* cRNA was synthesized with the mMESSAGE mMACHINE T7 High Yield Capped RNA ULTRA Transcription Kit (Ambion), as described previously (Jozefkowicz *et al.*, 2013). The synthesized products were resuspended in RNAase free water. The cRNA integrity was checked on agarose gel and quantified in a NanoDrop™ 2000 (Thermo Fisher Scientific).

Defolliculated *Xenopus laevis* oocytes (stage V–VI) were micro injected with cRNAs and incubated in ND96 buffer (96 mM NaCl, 2 mM KCl, 1 mM $MgCl_2$, 1.8 mM $CaCl_2$, and 5 mM HEPES pH 7.5; ~ 200 mOsmol kg^{-1} H_2O) for 3 days at 18°C. The osmotic water permeability coefficient (P_f) of oocytes injected or noninjected (NI) with cRNA was determined by measuring the oocyte swelling rate in response to ND96 buffer diluted fivefold with distilled water, as explained previously (Fortuna *et al.*, 2019). For pH inhibition experiments, the oocyte internal proton concentration was modified as explained previously (Bellati *et al.*, 2010), and the swelling response was induced by transferring the oocytes to an incubation solution diluted fivefold with

distilled water. Briefly, oocytes were pre-incubated in solutions of different pH (MES for the 5.8 to 6.7 pH interval and HEPES for the 7.0 to 7.5 pH interval) containing 50 mM sodium acetate, 20 mM MES or HEPES, and supplemented with 1 M mannitol to adjust the osmolarity to ~200 mOsmol kg^{-1} H_2O. To calculate the final internal pH in oocytes treated with acetate buffers, we used the calibration curve performed by Bellati *et al.* (2010). Noninjected oocytes, pre-incubated in a pH 7.5 solution for pH experiments, were used as negative controls. All osmolarities were measured in a vapor pressure osmometer (5600C Wescor Inc., Logan, USA).

Bioinformatic analysis of *Zm*VAP proteins

Protein domains were identified with the Simple Modular Architecture Research Tool, SMART (Schultz *et al.*, 1998). Maize proteins containing a MSD domain were found in the B73 reference genome (RefGen_v4) via a BLAST with the *Zm*VAP27-1 MSD, and also were found in the SMART data base. *Zm*VAP27 homologous gene families were identified in the Monocots PLAZA 4.0 platform (Van Bel *et al.*, 2018). For the phylogenetic tree, to obtain a harmonic representation of the different plant species, the protein sequences were retrieved from the family HOM04000421 (Monocots data base), Dicots PLAZA 4.0, and Gymno PLAZA 1.0. Multiple sequence alignments (MSA) were assembled in the GUIDANCE2 server (Sela *et al.*, 2015) using the MAFFT (FFT-NS-100) algorithm. Unreliable sequences below a 0.60 confidence score were removed and the alignment redone. The sequences were trimmed with TrimAl (Capella-Gutierrez *et al.*, 2009) removing unreliable columns below a 0.80 confidence score conserving 35% of the sequence. The best-fit model was found using ModelFinder (Kalyaanamoorthy *et al.*, 2017) implemented in the IQ-TREE (version 1.10) Phylogenomic software. Branch support was calculated with the ultrafast bootstrap (Hoang *et al.*, 2018) and the SH-aLRT branch test (Guindon *et al.*, 2010). The best-fit model was JTT+F+R7. Trees were edited using the Interactive Tree of Life tool (Letunic & Bork, 2016). *Zm*VAP transcriptomic data was obtained and analyzed in the platform GENEVESTIGATOR® v4 (https://genevestigator.com) (Zimmermann *et al.*, 2004).

Results

Identification of *Zm*PIP2;5 interactors associated with the cytoskeleton

We previously reported that *Zm*PIP2;5 physical interaction with the syntaxin SYP121 regulates its subcellular trafficking and water transport activity (Besserer *et al.*, 2012). To identify other *Zm*PIP2;5 partners we designed a pull-down assay using BMS suspension cells. We generated transgenic lines that overexpressed YFP-*Zm*PIP2;5 under the control of the 35S promoter and selected lines with high and stable protein expression levels. Confocal microscopy analysis showed that YFP-*Zm*PIP2;5 was localized in the PM (Fig. **1a**). We then determined the cell membrane P_f by protoplast swelling assays and observed that the P_f was greater in the *Zm*PIP2;5 overexpression cells compared with wild type cells (Fig. **1b**), demonstrating that YFP-*Zm*PIP2;5 was a functional water channel in these cells. We used this YFP-*Zm*PIP2;5 overexpression cell line and a cell line overexpressing YFP (negative control) to perform a pull-down assay. With a *P*-like value < 0.05 and fold change (FC) > 2, 138 proteins were defined as putative *Zm*PIP2;5 interactors (Table S3). Then, we created a shorter interest list, which also included some proteins with a FC > 1.5 (Table 1).

A cellulose synthase subunit (CESA) was pulled-down with *Zm*PIP2;5, similarly to what was reported in a previous pull-down assay with *At*PIP2;1 (Bellati *et al.*, 2016). Interestingly, the CESA complex is one of the few identified mediators of the interaction between the PM and cortical microtubules (Krtková *et al.*, 2016), the latter guiding cellulose deposition (Paredez *et al.*, 2006). Then, we hypothesized that PIPs may also interact with the cytoskeleton, and that this interaction may underlie specific events regulating PIP function in cell water and/or solute homeostasis. In support of this hypothesis, (i) we observed the pull-down of proteins involved in PM-cytoskeleton association together with *Zm*PIP2;5 (Table 1), (ii) in a previous pull-down assay using *Zm*PIP2;6 as bait, we identified kinesin, dynamin, actin, and tubulin as putative interactors (Hachez *et al.*, 2014a, Table S4), and (iii) the reported *At*PIP2;1 pull-down assay also identified several dynamin and tubulin isoforms as interactors (Bellati *et al.*, 2016, Table S4). Remarkably, we also identified two members of the plant-specific Networked (NET) actin-binding proteins superfamily (Deeks *et al.*, 2012), and two VAPs, *Zm*VAP27-1 and *Zm*VAP27-2. VAPs and NETs, together with the cytoskeleton, are involved in EPCSs organization (Wang *et al.*, 2014). This evidence points to an association of the PM-localized *Zm*PIP2;5 with the cortical cytoskeleton and ER, possibly through an interaction with *Zm*VAP27-1 and *Zm*VAP27-2. Therefore, we decided to investigate the interaction between PIPs and VAP27s and its functional implications.

*Zm*PIP2;5 interacts with *Zm*VAP27 proteins

To confirm *Zm*PIP2;5 interaction with *Zm*VAP27-1 and *Zm*VAP27-2, we performed a yeast SUS. The cDNAs of *Zm*VAP27-1 and *Zm*VAP27-2 were cloned using BMS cell total RNA as a template. *Zm*VAP27s were N-terminal tagged with NubG (prey) and *Zm*PIP2;5 was C-terminal tagged with Cub-PLV (bait). NubG and NubWT fragments served as negative and positive controls of the Nub-Cub interaction, respectively (Grefen *et al.*, 2009). The specificity in the interaction was observed by reducing bait protein expression with methionine, which inhibits the *met25* promoter. Yeast growth was observed when *Zm*PIP2;5-Cub-PVL was expressed with both VAP27 proteins or with the positive NubWT control, whereas it was not observed for the negative control (Fig. **2a**), indicating that *Zm*PIP2;5 is able to physically interact with *Zm*VAP27-1 or *Zm*VAP27-2. Bait and prey protein expression in the transformed yeast was confirmed by immunoblots (Fig. **2b**).

Additionally, the physical interaction between *Zm*PIP2;5 and *Zm*VAP27s was validated by a BiFC assay using the *pBiFCt-2in1* vector (Grefen & Blatt, 2012). This vector carries each protein of interest in frame with half of the YFP protein (YFPn and YFPc) and a soluble monomeric red fluorescent protein (mRFP1) as an internal transformation and expression control. *Zm*SYP121 and *Np*PMA2 were used as the positive and negative *Zm*PIP2;5 interaction control, respectively (Besserer *et al.*, 2012). The constructs were agro-infiltrated in *N. benthamiana* leaves and the fluorescence was observed by confocal microscopy after three days. For both the YFPn-*Zm*PIP2;5/YFPc-*Zm*VAP27-1 and YFPn-*Zm*PIP2;5/YFPc-*Zm*VAP27-2 pairs, a YFP fluorescent signal was detected with a particular bright dot pattern (insets Fig. **2c**). As expected, a YFP fluorescent signal was also observed when YFPn-*Zm*PIP2;5 was co-expressed with YFPc-*Zm*SYP121, whereas no signal was observed when YFPn-*Zm*PIP2;5 was co-expressed with YFPc-*Np*PMA2 (Fig. **2c**). Additionally, we tested the specificity of the interaction between *Zm*VAP27s and *Zm*PIP2;5 by analyzing the YFPn-*Zm*VAP27-1/YFPc-*Np*PMA2 pair, and did not detect any YFP signal, indicating that *Zm*VAP27-1 is not broadly interacting with all PM proteins (Fig. **S1**). Altogether, the assays in the yeast heterologous system and in plant cells confirmed the pull-down data showing that *Zm*VAP27-1 and *Zm*VAP27-2 interact with *Zm*PIP2;5.

The MSD of VAP27s is required for PIP2-VAP27 interaction

Both *Zm*VAP27-1 and *Zm*VAP27-2 present the three characteristic VAP protein domains (Wang *et al.*, 2016): the cytoplasmic major sperm domain (MSD), the coiled-coil domain (CCD), and the transmembrane domain (TMD) that anchors the protein to the ER (Fig. **3a**). To determine which domain is involved in the interaction with *Zm*PIP2;5, we generated *Zm*VAP27-1 mutants and tested their physical interaction with *Zm*PIP2;5 by means of BiFC assays. Ratiometric fluorescence quantification resulted in a significant increase in the YFP/RFP ratio when the MSD was present in *Zm*VAP27-1 (i.e. for the pairs YFPn-*Zm*PIP2;5/YFPc-*Zm*VAP27-1, YFPn-*Zm*PIP2;5/YFPc-*Zm*VAP27-1ΔTMD, and YFPn-*Zm*PIP2;5/YFPc-*Zm*VAP27-1ΔCCD), whereas the YFP/RFP ratio of the cells expressing YFPn-*Zm*PIP2;5/YFPc-*Zm*VAP27-1ΔMSD was not significantly different from the negative control (Fig. **3b**, representative confocal images in Fig. **S2a**). The expression of *Zm*VAP27-1ΔMSD was confirmed by confocal microscopy in tobacco leaves transiently expressing mTRQ2 tagged protein (Fig. **S2b**). Altogether, these data suggest that the VAP27 MSD domain is required for their interaction with *Zm*PIP2;5.

PIP2 C-terminal domain is not required for PIP2-VAP27 interaction

Most of the reported VAP interactors are cytoplasmic proteins with a binding motif of two phenylalanines in an acidic tract (FFAT) or a FFAT-like motif (Murphy & Levine, 2016). Using a mammal and yeast VAP interactome, an algorithm to predict VAP binding motifs was proposed (Murphy & Levine, 2016). We tested *Zm*PIP2;5 cytoplasmic domains with that algorithm and found no putative interaction motifs within these sequences. However, this algorithm also predicted a weak interaction of the mammalian potassium channel Kv2.1, which is known to interact with VAP proteins through a non-canonical C-terminal domain binding motif that is rich in serine residues (Johnson *et al.*, 2018). As the *Zm*PIP2;5 C-terminus is also serine rich, we tested whether this domain was required for the interaction with *Zm*VAP27-1. We generated the *Zm*PIP2;5ΔC deletion mutant and tested its physical interaction with *Zm*VAP27-1 by means of BiFC assays. The *Zm*PIP2;5ΔC mutant still interacted with *Zm*VAP27-1 (Fig. **3b** and Fig. **S2a**), suggesting that another *Zm*PIP2;5 cytosolic domain should be involved in the interaction with *Zm*VAP27-1.

***Zm*PIP2;5 and *Zm*VAP27s are in close vicinity in EPCS and endocytic structures**

To study VAP27 protein intracellular localization relative to the localization of *Zm*PIP2;5, *Zm*VAP27-1 or *Zm*VAP27-2 and *Zm*PIP2;5 were tagged with mTRQ2 and mVenus, respectively, and transiently expressed in *N. benthamiana* leaves. mTRQ2-*Zm*VAP signals were found close to the PM and around the nucleus in a reticular network, characteristic of the ER (Fig. **4a,b**). This was better observed in high magnification images, in which the mTRQ2-*Zm*VAP27-1 fluorescent signals were in the cortical ER structure near to the PM and in punctuated structures (Fig. **4c**), as previously described for *At*VAP27s present in EPCS (Wang *et al.*, 2014, 2016). The expression of both VAP27s did not modify *Zm*PIP2;5 PM localization (Fig. **4a,b**).

PIPs are internalized in response to salt stress (Boursiac *et al.*, 2005; Prak *et al.*, 2008; Pou *et al.*, 2016; Ueda *et al.*, 2016), and VAP27 proteins are involved in endocytic traffic (Stefano *et al.*, 2018). To obtain insights into the nature of the contact between *Zm*VAP27-1 with *Zm*PIP2;5, we challenged the cells with a short but strong hyperosmotic salt stress, aiming to plasmolyze the cells but also to observe endocytosis. After 15 min in 4% NaCl, protoplast detachment from the cell wall occurred and both proteins were detected in Hechtian strands (arrows, Fig. **4d**,**f** and Fig. **S3**), which connect the cell wall to the protoplast (Lang-Pauluzzi & Gunning, 2000). Interestingly, characteristic endocytosed intracellular vesicles containing the aquaporin in response to NaCl were surrounded by the mTRQ2-*Zm*VAP27-1 signal (arrows, Fig. **4e**,**g**).

To further investigate the interaction between *Zm*PIP2;5 and *Zm*VAP27-1 we used the Airyscan confocal microscope super-resolution module (Zeiss LSM710). This approach revealed a patched arrangement of mVenus-*Zm*PIP2;5 in the PM (Fig. **5a**), suggesting that *Zm*PIP2;5 organizes in PM domains as previously shown for *At*PIP2;1 (Li *et al.*, 2011). This irregular pattern colocalized partially with the nested arrangement of *Zm*VAP27-1 in the ER (Fig. **5a**). Regarding the mVenus-*Zm*PIP2;5-labelled intracellular vesicles that were near to the PM, we were not able to observe mTRQ2 and mVenus signal colocalization (Fig. **5b**). Cell membrane reorganization upon NaCl treatment highlighted mVenus-*Zm*PIP2;5 and mTRQ2-*Zm*VAP27-1 colocalization in Hechtian strands (Fig. **5c,f**, zoom out of this panel in Fig. **S3b)** and *Zm*PIP2;5-labelled vesicles (Fig. **5d**,**g)**, as already shown. Also, we detected colocalization of both proteins in globular structures (Fig. **5e,h**), which resemble the PM invaginations labelled with Venus-*At*PIP2;7 induced in response to salt stress conditions (Pou *et al.*, 2016). Additional images showing mVenus-*Zm*PIP2;5 and mTRQ2-*Zm*VAP27-1 colocalization upon NaCl stress are shown in Fig. **S4**.

Altogether, these data suggested that *Zm*VAP27-1-labelled ER is organized close to the different structures involved in *Zm*PIP2;5 internalization.

*Zm*VAP27-1 positively modifies the osmotic membrane water permeability of *Zm*PIP2;5 expressing oocytes

To determine whether *Zm*VAP27-1 expression modified *Zm*PIP2;5 water transport activity, we performed *Xenopus* oocyte swelling assays. Both *Zm*PIP2;5 and *Zm*VAP27-1 coding cRNAs were injected in oocytes and, after three days, the latter were subjected to hypo-osmotic shock. The P_f values of oocytes injected with *ZmVAP27-1* cRNA alone were not different from the P_f of NI oocytes, whereas a significant P_f increase was observed when the oocytes were injected with *ZmPIP2;5* cRNA. *ZmPIP2;5* and *ZmVAP27-1* cRNA co-injection in a 1:1 ratio did not modify the mean P_f value in comparison with *Zm*PIP2;5 expression alone. However, the co-injection of *Zm*PIP2;5 and *Zm*VAP27-1 cRNA in a 1:10 ratio caused a mean P_f value increase over 35% (Fig. **6a**, Fig. **S5a,b**), indicating a positive synergistic effect on the cell water permeability.

The water permeation through PIP pores is regulated by the cytosolic proton concentration ($[H^+]_i$) (Tournaire-Roux *et al.*, 2003). Under acid conditions, residues located in cytosolic loop D are protonated, and concomitant loop reorganization leads to PIP pore closure (Törnroth-Horsefield *et al.*, 2006; Frick *et al.*, 2013). A P_f vs $[H^+]_i$ sigmoidal curve characterizes the cooperative behavior in proton sensing of the channels that integrate the tetramer (Bellati *et al.*, 2010; Yaneff *et al.*, 2014; Jozefkowicz *et al.*, 2016). To evaluate if the PIP-VAP27 interaction affected proton sensing, as it may involve PIP cytosolic domains, we compared the relative-P_f vs $[H^+]_i$ curves for *Zm*PIP2;5 expressed alone and co-expressed with *Zm*VAP27-1 (1:10) (Fig. **6b**, absolute P_f values reported in Fig. **S5c,d**). The $[H^+]_{0.5}$ remained constant among the assays (0.21 + 0.02 vs 0.24 + 0.01, mean + SE, n = 2), suggesting that the interaction among *Zm*PIP2;5 and *Zm*VAP27-1 did not alter the aquaporin structural elements involved in pH sensing.

The PIP2-VAP27 interaction is conserved among different angiosperms

Currently our understanding about plant VAPs mainly arises from research in the plant model Arabidopsis (Wang *et al.*, 2014; Pérez-Sancho *et al.*, 2015; Wang *et al.*, 2016), whereas maize

VAP proteins have not been characterized yet. Intending to better understand the PIP-VAP27 interaction we identified maize VAPs and studied VAP27 phylogeny in green plants (*Viridiplantae*). We identified 19 proteins containing a MSD in the B73 maize genome (Fig. **S6a**). The MSD is a conserved feature among VAPs, but proteins from other families may also contain this domain. Indeed, 17 of the 19 proteins were homologues of the previously characterized *At*VAP27s, whereas the remaining two proteins were non-related to VAP27s. The *Zm*PIP2;5 interactors (*Zm*VAP27-1 and *Zm*VAP27-2) are part of the same homology group with an MSD amino acid sequence identity over 50% (Fig. **S6b**). Publicly available transcriptome data analysis showed that six of 14 group members are highly expressed in most plant tissues (Fig. **S6c**). Both *Zm*VAP27-1 and *Zm*VAP27-2 are among these highly expressed genes, and exhibit the greatest expression levels in roots (Fig. **S6c**), similar to *Zm*PIP2;5 (Hachez *et al.*, 2006, 2008).

To obtain insights into the family evolution of the *Zm*VAP27-1 and *Zm*VAP27-2 homology group, we performed a phylogenetic analysis. A balanced selection of species and genes allowed an alignment of 254 proteins from 41 green plant species (see Material and Methods section). The reconstructed phylogenetic tree showed that this VAP27 homology group can be further subdivided into two paralog groups (Fig. **7a**, the full phylogeny is shown in Fig. **S7**), which correspond with the previously defined *At*VAP27s clade I and III (Wang *et al.*, 2016). The presence of these clades can be traced back to Gymnosperms, suggesting that both clades were present in the Spermatophyta ancestor. Within each of these two main clades, two subgroups can be distinguished for Angiosperms, showing family-specific expansion events. *Zm*VAP27-1, together with other seven *Zm*VAP27s, clearly group in the *At*VAP27 clade I, the closer Arabidopsis *Zm*VAP27-1 orthologs being the isoforms *At*VAP27-1/3/5/7. On the other hand, *Zm*VAP27-2, and five other *Zm*VAP27s, group with the *At*VAP27 clade III, the closer Arabidopsis *Zm*VAP27-2 ortholog being the isoform *At*VAP27-2 (Fig. **7a**).

Regarding PIP2 channels evolution, their origin can be traced back to the Embryophyta ancestor (Soto *et al.*, 2012; Abascal *et al.*, 2014). We hypothesized that the PIP2-VAP27 interaction is conserved through evolution. We looked for evidence to support this hypothesis in the published Arabidopsis data. We localized in the Arabidopsis Interactome Map (Consortium, 2011) *At*VAP27-1 interaction with *At*PIP2;3, *At*PIP2;7, and *At*PIP2;8 and the interaction of *At*VAP27-4 with *At*PIP2;7. Also, the *At*VAP27-3 isoform was pulled-down with *At*PIP2;1 and not with *At*PIP1;2 (Bellati *et al.*, 2016). We validated the interaction between *At*PIP2;7 and *At*VAP27-

1 by BiFC (Fig. **7b**), and we also tested whether *At*PIP2;7 was able to interact with *Zm*VAP27-1. As observed in Fig. **7b**, co-expression of both proteins led to a fluorescent signal, demonstrating their interaction. Altogether, these data showed that the PIP2-VAP27 interaction is an ancient land plant feature, being at least present in the common Angiosperm ancestor. Future work will elucidate whether this interaction is also present in bryophytes, or if it is a distinctive vascular plant feature.

Discussion

To unravel the different aquaporin roles and regulation mechanisms in water and/or solute homeostasis in plant cells, it is crucial to identify their intracellular partners. The pull-down assays presented here together with previous assays using tagged PIPs (Hachez *et al.*, 2014a; Bellati *et al.*, 2016) allowed protein identification from the cytoskeleton and ER as PIPs partners (Table S4), suggesting a close interaction between PIPs and those cellular structures. Moreover, we showed that PIP2s and the ER resident VAP27s interact, and presented novel evidence of plant aquaporin activity regulation by EPC residents.

To our knowledge, *Zm*PIP2;5 is the first plant PM protein identified as a partner of ER located VAP27s. We confirmed these interactions by SUS and BiFC experiments (Fig. **2**). Interestingly, ER located VAP27s are anchored to the cell wall by unknown PM proteins (Wang *et al.*, 2016). We speculate that *Zm*PIP2;5 might be one of the proteins anchoring ER-located *Zm*VAP27s to the cell wall. Actually, the cell wall restricts *At*PIP2;1 mobility (Martiniere *et al.*, 2012) and, using fluorescence recovery after photobleaching assays (Methods S2), we also showed that *Zm*PIP2;5 mobility in the PM is restricted in comparison with other proteins that expose few amino acids to the apoplast, like *Zm*LTi6A (Fig. **S8**). Also, we demonstrated that the *Zm*VAP27-1 MSD is essential for the PIP-VAP27 interaction, whereas the CCD and TMD are not (Fig. **3b**). It is important to point out that *Zm*PIP2;5 and *Zm*SYP121 are both PM residents and their BiFC signals reconstitute at the PM, whereas the BiFC signal of the *Zm*PIP2;5-*Zm*VAP27-1/2 pairs reconstitutes in dotted structures (Fig. **2c**), reminiscent of the *At*VAP27-1 bright dotted pattern (Wang *et al.*, 2016). On the other hand, mTRQ2-*Zm*VAP27-1/2 expression in the ER did not prevent mVenus-*Zm*PIP2;5 PM localization (Fig. **4** and **5**). These results, together with the central role of the MSD in the interaction, demonstrate that the interaction between VAP27-1/2 and

*Zm*PIP2;5 occurs at EPCSs. We also showed that *At*VAP27-1 interacted with *At*PIP2;7 (Fig. **7**), and *At*VAP27-3 was also detected in an *At*PIP2;1 interactomic study performed by Bellati *et al.* (2016). All these observations with the fact that *Zm*VAP27-1 was not interacting with the H^+-ATPase PMA2 in BiFC assays (Fig. **S1**), another protein that is enriched in PM microdomains just like PIP channels (Laloi *et al.*, 2007), might indicate that PIP aquaporins play a role in anchoring the EPCSs to the cell wall.

Endocytosis is a rapid way to adjust PIP protein abundance in the PM in response to an osmotic or salt stress (Chaumont & Tyerman, 2014; Pou *et al.*, 2016). Salt stress induced *At*PIP2;1 internalization is a process that depends on two kinases: phosphatidylinositol 3-kinase (PI3K) and phosphatidylinositol 4-kinase (PI4K) (Ueda *et al.*, 2016). Interestingly, *At*VAP27-1/3 bind with high affinity to different phosphorylated PI (Stefano *et al.*, 2018), among them the PI3K and PI4K products. In addition, endocytosis is partially impaired in the plant double mutant *vap27-1/vap27-3* (Stefano *et al.*, 2018), as it is impaired in mammal cells lacking VAPs (Dong *et al.*, 2016). Here, we showed that salt-stress induced vesicles carrying *Zm*PIP2;5 are wrapped with *Zm*VAP27-1-labelled ER (Fig. **4e**, **5d** and **5e**). Therefore, PIP interaction with VAP27s can facilitate PIP loading into endocytic structures enriched in specific PIs.

Upon osmotic stress, *At*PIP2;7 interaction with the tryptophan-rich sensory protein/translocator (TSPO) leads to aquaporin level reduction in the PM, through degradation by the autophagic pathway (Hachez *et al.*, 2014b; Jurkiewicz *et al.*, 2020). How the internalization of this complex occurs is still unknown. Interestingly, TSPO and PIP interaction occurs only if TSPO binds PI(4,5)P2 (Jurkiewicz *et al.*, 2020) and VAP27s also bind PI(4,5)P2 (Stefano *et al.*, 2018). Moreover, *At*VAP27-1 interacts with essential proteins involved in endocytic component autophagy (Wang & Hussey, 2019). As *At*PIP2;7 interacts with *At*VAP27-1 (Fig. **7b**), we propose that PIP autophagy may be initiated at EPCSs through its interaction with TSPO and VAP27s. This hypothesis will need to be addressed.

The PIP-VAP27 interaction increases oocyte membrane water permeability compared with oocytes expressing PIP alone (Fig. **6a**). And we found no evidence of a modification in PIP proton sensing by VAP27s (Fig. **6b**), suggesting that the structural elements involved in pH sensing are not affected by the interaction. Still, we cannot discard a conformational pore modification. Therefore, the P_f increase could be explained either by a greater intrinsic permeability of PIP channels due to a conducting pore conformational change, or by a greater active channel number

in the PM. Under normal conditions, when no stress signals are perceived by cells to induce PIP internalization, VAP27s could recruit and stabilize the channels in EPCSs similar to the VAPs clustering of the mammal potassium channel Kv2.1 (Kirmiz *et al.*, 2018). Interestingly, cells with genetically elevated PI(4,5)P2 levels also have greater P_f than control cells (Ma *et al.*, 2015). The authors were able to link the PI effect on P_f to aquaporins, but they were not able to discern between an increase in channel abundance in the PM or an increase in their water channel activity. Further research will help to understand if VAP27s stabilize PIPs in the PM and guide the channels to rapid endocytosis in response to a stimulus.

We recently reported how *Zm*PIP2;5 expression levels affect water relations and plant growth (Ding *et al.*, 2020). *Zm*PIP2;5 is the most highly expressed PIP2 isoform in roots. Interestingly, the two different *Zm*VAP27s that interact with *Zm*PIP2;5 are also highly expressed in roots (Fig. **S6c**), and belong to different clades that we traced back to the Spermatophyta ancestor (*c.* 319 million year ago, Jiao *et al.*, 2011) (Fig. **7a**). The challenge of future research will be to understand (i) the role of the interaction in plant water movement, especially in response to osmotic and salt stress, (ii) whether these interactions are linked to the acquisition of new functionalities *in planta*, and (iii) whether the *Zm*PIP2;5/*Zm*VAP27-1 and *Zm*PIP2;5/*Zm*VAP27-2 interactions form part of different EPCSs types or not.

Acknowledgements

We thank MASSPROT, IMABIOL, Marie-Christine Eloy for confocal expertise and Joseph Nader for his helpful advice in benchwork. This work was supported by the Belgian National Fund for Scientific Research (FNRS, FRFC 2.4.501.06F), the "Communauté française de Belgique-Actions de Recherches Concertées" (grants ARC16/21-075), the Pierre and Colette Bauchau Award, the Consejo Nacional de Investigaciones Científicas y Técnicas (CONICET PIP 2014-0206), and the Agencia Nacional de Promoción Científica y Tecnológica (PICT 2017-0244). A.R.F. was supported by an Incoming Post-doc Move-in Louvain Fellowship co-funded by the Marie Curie Actions. F.S. was supported by a research fellow at the Universidad de Buenos Aires. T.L. was supported by a research fellow at the Fonds de Formation à la Recherche dans l'Industrie et l'Agriculture.

Author contributions: A.R.F. and F.C. designed the experiments. A.R.F., T.L., F.S., K.F., and H.D. performed the experiments. A.R.F, T.L, F.S., H.D., P.M., K.A., and F.C. analyzed the data. A.R.F. and F.C. wrote the manuscript. All the authors contributed to the discussion and revision of the manuscript.

References

Abascal F, Irisarri I, Zardoya R. **2014**. Diversity and evolution of membrane intrinsic proteins. *Biochimica et Biophysica Acta* **1840**: 1468–1481.

Afzal Z, Howton T, Sun Y, Mukhtar M. **2016**. The roles of aquaporins in plant stress responses. *Journal of Developmental Biology* **4**: 9.

Batoko H, Zheng H-Q, Hawes C, Moore I. **2000**. A Rab1 GTPase is required for transport between the endoplasmic reticulum and golgi apparatus and for normal golgi movement in plants. *The Plant Cell* **12**: 2201.

Bellati J, Alleva K, Soto G, Vitali V, Jozefkowicz C, Amodeo G. **2010**. Intracellular pH sensing is altered by plasma membrane PIP aquaporin co-expression. *Plant Molecular Biology* **74**: 105–118.

Bellati J, Champeyroux C, Hem S, Rofidal V, Krouk G, Maurel C, Santoni V. **2016**. Novel aquaporin regulatory mechanisms revealed by interactomics. *Molecular & Cellular Proteomics* **15**: 3473–3487.

Besserer A, Burnotte E, Bienert GP, Chevalier AS, Errachid A, Grefen C, Blatt MR, Chaumont F. **2012**. Selective regulation of maize plasma membrane aquaporin trafficking and activity by the SNARE SYP121. *The Plant Cell* **24**: 3463.

Bienert GP, Heinen RB, Berny MC, Chaumont F. **2014**. Maize plasma membrane aquaporin *Zm*PIP2;5, but not *Zm*PIP1;2, facilitates transmembrane diffusion of hydrogen peroxide. *Biochimica et Biophysica Acta - Biomembranes* **1838**: 216–222.

Boursiac Y, Chen S, Luu D-T, Sorieul M, van den Dries N, Maurel C. **2005**. Early effects of salinity on water transport in Arabidopsis roots. Molecular and cellular features of aquaporin expression. *Plant Physiology* **139**: 790–805.

Bradford MM. **1976**. A rapid and sensitive method for the quantitation of microgram quantities of protein utilizing the principle of protein-dye binding. *Analytical Biochemistry* **72**: 248–254.

Capella-Gutierrez S, Silla-Martinez JM, Gabaldon T. **2009**. trimAl: a tool for automated alignment trimming in large-scale phylogenetic analyses. *Bioinformatics* **25**: 1972–1973.

Chaumont F, Tyerman SD. **2014**. Aquaporins: highly regulated channels controlling plant water relations. *Plant Physiology* **164**: 1600–1618.

Chevalier AS, Bienert GP, Chaumont F. **2014**. A new LxxxA motif in the transmembrane Helix3 of maize aquaporins belonging to the plasma membrane intrinsic protein PIP2 group is required for their trafficking to the plasma membrane. *Plant Physiology* **166**: 125–138.

Consortium AIM. **2011**. Evidence for network evolution in an Arabidopsis interactome map. *Science* **333**: 601–607.

Deeks MJ, Calcutt JR, Ingle EKS, Hawkins TJ, Chapman S, Richardson AC, Mentlak DA, Dixon MR, Cartwright F, Smertenko AP, *et al.* 2012. A superfamily of actin-binding proteins at the actin-membrane nexus of higher plants. *Current Biology* **22**: 1595–1600.

Ding L, Milhiet T, Couvreur V, Nelissen H, Meziane A, Parent B, Aesaert S, Lijsebettens MV, Inzé D, Tardieu F, *et al.* 2020. Modification of the expression of the aquaporin *Zm*PIP2;5 affects water relations and plant growth. *Plant Physiology* **182**: 2154-2165.

Dong R, Saheki Y, Swarup S, Lucast L, Harper JW, De Camilli P. **2016**. Endosome-ER contacts control actin nucleation and retromer function through VAP-dependent regulation of PI4P. *Cell* **166**: 408–423.

Fortuna AC, Palma GZD, Car LA, Armentia L, Vitali V, Zeida A, Estrin DA, Alleva K. **2019**. Gating in plant plasma membrane aquaporins: the involvement of leucine in the formation of a pore constriction in the closed state. *The FEBS Journal* **286**: 3473–3487.

Fox AR, Maistriaux LC, Chaumont F. **2017**. Toward understanding of the high number of plant aquaporin isoforms and multiple regulation mechanisms. *Plant Science* **264**: 179–187.

Frick A, Järvå M, Törnroth-Horsefield S. **2013**. Structural basis for pH gating of plant aquaporins. *FEBS Letters* **587**: 989–993.

Glaab E, Schneider R. **2015**. RepExplore: addressing technical replicate variance in proteomics and metabolomics data analysis. *Bioinformatics* **31**: 2235–2237.

Goldman A, Harper S, Speicher DW. **2016**. Detection of proteins on blot membranes. *Current Protocols in Protein Science* **86**: 10.8.1-10.8.11.

Gorgoni B, Fiorentino L, Marchioni M, Carnevali F. **1995**. Cloning, expression and functional role of XRPFI α and β Subunits in *Xenopus laevis* oocyte. *Biochemical and Biophysical Research Communications* **215**: 1088–1095.

Grefen C, Blatt MR. **2012**. A 2in1 cloning system enables ratiometric bimolecular fluorescence complementation (rBiFC). *BioTechniques* **53**: 311–314.

Grefen C, Obrdlik P, Harter K. **2009**. The determination of protein-protein interactions by the mating-based split-ubiquitin system (mbSUS). *Methods in Molecular Biology (Clifton, N.J.)* **479**: 217–233.

Grondin A, Rodrigues O, Verdoucq L, Merlot S, Leonhardt N, Maurel C. **2015**. Aquaporins contribute to ABA-triggered stomatal closure through OST1-mediated phosphorylation. *The Plant Cell* **27**: 1945–1954.

Guindon S, Dufayard J-F, Lefort V, Anisimova M, Hordijk W, Gascuel O. **2010**. New algorithms and methods to estimate maximum-likelihood phylogenies: assessing the performance of PhyML 3.0. *Systematic Biology* **59**: 307–321.

Hachez C, Heinen RB, Draye X, Chaumont F. **2008**. The expression pattern of plasma membrane aquaporins in maize leaf highlights their role in hydraulic regulation. *Plant Molecular Biology* **68**: 337.

Hachez C, Laloux T, Reinhardt H, Cavez D, Degand H, Grefen C, Rycke RD, Inzé D, Blatt MR, Russinova E, *et al.* 2014a. Arabidopsis SNAREs SYP61 and SYP121 coordinate the trafficking of plasma membrane aquaporin PIP2;7 to modulate the cell membrane water permeability. *The Plant Cell* **26**: 3132–3147.

Hachez C, Moshelion M, Zelazny E, Cavez D, Chaumont F. **2006**. Localization and quantification of plasma membrane aquaporin expression in maize primary root: A clue to understanding their role as cellular plumbers. *Plant Molecular Biology* **62**: 305–323.

Hachez C, Veljanovski V, Reinhardt H, Guillaumot D, Vanhee C, Chaumont F, Batoko H. **2014b**. The Arabidopsis abiotic stress-induced TSPO-related protein reduces cell-surface expression of the aquaporin PIP2;7 through protein-protein interactions and autophagic degradation. *The Plant Cell* **26**: 4974–4990.

Hecker A, Wallmeroth N, Peter S, Blatt MR, Harter K, Grefen C. **2015**. Binary 2in1 vectors improve *in planta* (co)localization and dynamic protein interaction studies. *Plant Physiology* **168**: 776–787.

Heinen RB, Ye Q, Chaumont F. **2009**. Role of aquaporins in leaf physiology. *Journal of Experimental Botany* **60**: 2971–2985.

Hoang DT, Chernomor O, von Haeseler A, Minh BQ, Vinh LS. **2018**. UFBoot2: improving the ultrafast bootstrap approximation. *Molecular Biology and Evolution* **35**: 518–522.

Hosy E, Martinière A, Choquet D, Maurel C, Luu D-T. **2015**. Super-resolved and dynamic imaging of membrane proteins in plant cells reveal contrasting kinetic profiles and multiple confinement mechanisms. *Molecular Plant* **8**: 339–342.

Jiao Y, Wickett NJ, Ayyampalayam S, Chanderbali AS, Landherr L, Ralph PE, Tomsho LP, Hu Y, Liang H, Soltis PS, *et al.* 2011. Ancestral polyploidy in seed plants and angiosperms. *Nature* **473**: 97–100.

Johnson B, Leek AN, Solé L, Maverick EE, Levine TP, Tamkun MM. **2018**. Kv2 potassium channels form endoplasmic reticulum/plasma membrane junctions via interaction with VAPA and VAPB. *Proceedings of the National Academy of Sciences* **115**: E7331–E7340.

Jozefkowicz C, Rosi P, Sigaut L, Soto G, Pietrasanta LI, Amodeo G, Alleva K. **2013**. Loop A is critical for the functional interaction of two *Beta vulgaris* PIP aquaporins. *PLoS ONE* **8**: e57993.

Jozefkowicz C, Sigaut L, Scochera F, Soto G, Ayub N, Pietrasanta LI, Amodeo G, González Flecha FL, Alleva K. **2016**. PIP water transport and its pH dependence are regulated by tetramer stoichiometry. *Biophysical Journal* **110**: 1312–1321.

Jurkiewicz P, Senicourt L, Ayeb H, Lequin O, Lacapere J-J, Batoko H. **2020**. A plant-specific N-terminal extension reveals evolutionary functional divergence within translocator proteins. *iScience* **23**: 100889.

Kalyaanamoorthy S, Minh BQ, Wong TKF, von Haeseler A, Jermiin LS. **2017**. ModelFinder: fast model selection for accurate phylogenetic estimates. *Nature Methods* **14**: 587–589.

Kim H, Kwon H, Kim S, Kim MK, Botella MA, Yun HS, Kwon C. **2016**. Synaptotagmin 1 negatively controls the two distinct immune secretory pathways to powdery mildew fungi in Arabidopsis. *Plant and Cell Physiology* **57**: 1133–1141.

Kirmiz M, Vierra NC, Palacio S, Trimmer JS. **2018**. Identification of VAPA and VAPB as Kv2 channel-interacting proteins defining endoplasmic reticulum-plasma membrane junctions in mammalian brain neurons. *The Journal of Neuroscience* **38**: 7562–7584.

Krtková J, Benáková M, Schwarzerová K. **2016**. Multifunctional microtubule-associated proteins in plants. *Frontiers in Plant Science* **7**: 474.

Laloi M, Perret A-M, Chatre L, Melser S, Cantrel C, Vaultier M-N, Zachowski A, Bathany K, Schmitter J-M, Vallet M, *et al.* 2007. Insights into the role of specific lipids in the formation and delivery of lipid microdomains to the plasma membrane of plant cells. *Plant Physiology* **143**: 461–472.

Lang-Pauluzzi I, Gunning BES. **2000**. A plasmolytic cycle: The fate of cytoskeletal elements. *Protoplasma* **212**: 174–185.

Lee HK, Cho SK, Son O, Xu Z, Hwang I, Kim WT. **2009**. Drought stress-induced Rma1H1, a RING membrane-anchor E3 ubiquitin ligase homolog, regulates aquaporin levels via ubiquitination in transgenic Arabidopsis plants. *The Plant Cell* **21**: 622–641.

Lee E, Vanneste S, Pérez-Sancho J, Benitez-Fuente F, Strelau M, Macho AP, Botella MA, Friml J, Rosado A. **2019**. Ionic stress enhances ER–PM connectivity via phosphoinositide-associated SYT1 contact site expansion in Arabidopsis. *Proceedings of the National Academy of Sciences* **116**: 1420–1429.

Letunic I, Bork P. **2016**. Interactive tree of life (iTOL) v3: an online tool for the display and annotation of phylogenetic and other trees. *Nucleic Acids Research* **44**: W242–W245.

Lewis JD, Lazarowitz SG. **2010**. Arabidopsis synaptotagmin SYTA regulates endocytosis and virus movement protein cell-to-cell transport. *Proceedings of the National Academy of Sciences* **107**: 2491–2496.

Li L, Wang H, Gago J, Cui H, Qian Z, Kodama N, Ji H, Tian S, Shen D, Chen Y, *et al.* 2015. Harpin Hpa1 interacts with aquaporin PIP1;4 to promote the substrate transport and photosynthesis in Arabidopsis. *Scientific Reports* **5**: 17207.

Li X, Wang X, Yang Y, Li R, He Q, Fang X, Luu D-T, Maurel C, Lin J. **2011**. Single-molecule analysis of PIP2;1 dynamics and partitioning reveals multiple modes of Arabidopsis plasma membrane aquaporin regulation. *The Plant Cell* **23**: 3780–3797.

Martiniere A, Lavagi I, Nageswaran G, Rolfe DJ, Maneta-Peyret L, Luu D-T, Botchway SW, Webb SED, Mongrand S, Maurel C, *et al.* 2012. Cell wall constrains lateral diffusion of plant plasma-membrane proteins. *Proceedings of the National Academy of Sciences* **109**: 12805–12810.

Maurel C, Boursiac Y, Luu D-T, Santoni V, Shahzad Z, Verdoucq L. **2015**. Aquaporins in plants. *Physiological Reviews* **95**: 1321–1358.

McFarlane HE, Lee EK, van Bezouwen LS, Ross B, Rosado A, Samuels AL. **2017**. Multiscale structural analysis of plant ER–PM contact sites. *Plant and Cell Physiology* **58**: 478–484.

Moshelion M, Moran N, Chaumont F. **2004**. Dynamic changes in the osmotic water permeability of protoplast plasma membrane. *Plant Physiology* **135**: 2301–2317.

Murphy SE, Levine TP. **2016**. VAP, a Versatile Access Point for the endoplasmic reticulum: Review and analysis of FFAT-like motifs in the VAPome. *Biochimica et Biophysica Acta - Molecular and Cell Biology of Lipids* **1861**: 952–961.

Paredez AR, Somerville CR, Ehrhardt DW. **2006**. Visualization of cellulose synthase demonstrates functional association with microtubules. *Science* **312**: 1491–1495.

Pérez-Sancho J, Tilsner J, Samuels AL, Botella MA, Bayer EM, Rosado A. **2016**. Stitching organelles: organization and function of specialized membrane contact sites in plants. *Trends in Cell Biology* **26**: 705–717.

Pérez-Sancho J, Vanneste S, Lee E, McFarlane HE, Valle AE del, Valpuesta V, Friml J, Botella MA, Rosado A. **2015**. The Arabidopsis synaptotagmin1 is enriched in endoplasmic reticulum-plasma membrane contact sites and confers cellular resistance to mechanical stresses. *Plant Physiology* **168**: 132–143.

Pou A, Jeanguenin L, Milhiet T, Batoko H, Chaumont F, Hachez C. **2016**. Salinity-mediated transcriptional and post-translational regulation of the Arabidopsis aquaporin PIP2;7. *Plant Molecular Biology* **92**: 731–744.

Prak S, Hem S, Boudet J, Viennois G, Sommerer N, Rossignol M, Maurel C, Santoni V. **2008**. Multiple phosphorylations in the C-terminal tail of plant plasma membrane aquaporins: Role in subcellular trafficking of *At* PIP2;1 in response to salt stress. *Molecular & Cellular Proteomics* **7**: 1019–1030.

Roche JV, Törnroth-Horsefield S. **2017**. Aquaporin protein-protein interactions. *International Journal of Molecular Sciences* **18**: 2255.

Schultz J, Milpetz F, Bork P, Ponting CP. **1998**. SMART, a simple modular architecture research tool: identification of signaling domains. *Proceedings of the National Academy of Sciences of the United States of America* **95**: 5857–5864.

Sela I, Ashkenazy H, Katoh K, Pupko T. **2015**. GUIDANCE2: accurate detection of unreliable alignment regions accounting for the uncertainty of multiple parameters. *Nucleic Acids Research* **43**: W7–W14.

Siao W, Wang P, Voigt B, Hussey PJ, Baluska F. **2016**. Arabidopsis SYT1 maintains stability of cortical endoplasmic reticulum networks and VAP27-1-enriched endoplasmic reticulum–plasma membrane contact sites. *Journal of Experimental Botany* **67**: 6161–6171.

Soto G, Alleva K, Amodeo G, Muschietti J, Ayub ND. **2012**. New insight into the evolution of aquaporins from flowering plants and vertebrates: orthologous identification and functional transfer is possible. *Gene* **503**: 165–176.

Stefano G, Renna L, Wormsbaecher C, Gamble J, Zienkiewicz K, Brandizzi F. **2018**. Plant endocytosis requires the ER membrane-anchored proteins VAP27-1 and VAP27-3. *Cell Reports* **23**: 2299–2307.

Takano J, Yoshinari A, Luu D-T. **2017**. Plant aquaporin trafficking. In: Chaumont F, Tyerman SD, eds. *Plant Aquaporins*. Cham: Springer International Publishing, 47–81.

Törnroth-Horsefield S, Wang Y, Hedfalk K, Johanson U, Karlsson M, Tajkhorshid E, Neutze R, Kjellbom P. **2006**. Structural mechanism of plant aquaporin gating. *Nature* **439**: 688–694.

Tournaire-Roux C, Sutka M, Javot H, Gout E, Gerbeau P, Luu D-T, Bligny R, Maurel C. **2003**. Cytosolic pH regulates root water transport during anoxic stress through gating of aquaporins. *Nature* **425**: 393–397.

Ueda M, Tsutsumi N, Fujimoto M. **2016**. Salt stress induces internalization of plasma membrane aquaporin into the vacuole in *Arabidopsis thaliana*. *Biochemical and Biophysical Research Communications* **474**: 742–746.

Valm AM, Cohen S, Legant WR, Melunis J, Hershberg U, Wait E, Cohen AR, Davidson MW, Betzig E, Lippincott-Schwartz J. **2017**. Applying systems-level spectral imaging and analysis to reveal the organelle interactome. *Nature* **546**: 162–167.

Van Bel M, Diels T, Vancaester E, Kreft L, Botzki A, Van de Peer Y, Coppens F, Vandepoele K. **2018**. PLAZA 4.0: an integrative resource for functional, evolutionary and comparative plant genomics. *Nucleic Acids Research* **46**: D1190–D1196.

Wang P, Hawkins TJ, Richardson C, Cummins I, Deeks MJ, Sparkes I, Hawes C, Hussey PJ. **2014**. The plant cytoskeleton, NET3C, and VAP27 mediate the link between the plasma membrane and endoplasmic reticulum. *Current Biology* **24**: 1397–1405.

Wang P, Richardson C, Hawkins TJ, Sparkes I, Hawes C, Hussey PJ. **2016**. Plant VAP27 proteins: domain characterization, intracellular localization and role in plant development. *New Phytologist* **210**: 1311–1326.

Wu XN, Rodriguez CS, Pertl-Obermeyer H, Obermeyer G, Schulze WX. **2013**. Sucrose-induced receptor kinase SIRK1 regulates a plasma membrane aquaporin in Arabidopsis. *Molecular & Cellular Proteomics* **12**: 2856–2873.

Yaneff A, Sigaut L, Marquez M, Alleva K, Pietrasanta LI, Amodeo G. **2014**. Heteromerization of PIP aquaporins affects their intrinsic permeability. *Proceedings of the National Academy of Sciences* **111**: 231–236.

Zelazny E, Miecielica U, Borst JW, Hemminga MA, Chaumont F. **2009**. An N-terminal diacidic motif is required for the trafficking of maize aquaporins ZmPIP2;4 and ZmPIP2;5 to the plasma membrane. *The Plant Journal* **57**: 346–355.

Zimmermann P, Hirsch-Hoffmann M, Hennig L, Gruissem W. **2004**. GENEVESTIGATOR. Arabidopsis microarray database and analysis toolbox. *Plant Physiology* **136**: 2621–2632.

Legends

Figure 1. Localization and activity of YFP-*Zm*PIP2;5 expressed in BMS cells. (a) Confocal images of maize Black Mexican Sweet (BMS) cells stably transformed with the *35S:YFP-ZmPIP2;5* construct. A clear colocalization of the YFP (green) and the plasma membrane dye FM4-64 (magenta) was observed. Scale bars, 10 μm. (b) Water permeability coefficient (P_f) values of non-transformed BMS cells (WT) and cells expressing YFP-*Zm*PIP2;5 (*Zm*PIP2;5OE). For each

scatter plot the lines indicate the mean + SE. The unpaired *t*-test was used to test the statistical difference between lines (***, $P < 0.001$).

Figure 2. *Zm*PIP2;5 interacts with *Zm*VAP27-1 and *Zm*VAP27-2. (a) Spilt-ubiquitin assay (SUS). Yeast coexpressing the *Zm*PIP2;5-Cub-PLV Met-repressible bait construct and the prey constructs NubG-*Zm*VAP27-1, NubG-*Zm*VAP27-2, NubG, or NubWT were dropped in a dilution series (OD 0.5, 0.05, and 0.005) onto synthetic media with or without 100 µM methionine to repress bait expression. Yeast growth was recorded after incubation for 48 h. This experiment was repeated with three independent transformed yeast lines for each construct pair. (b) Immunoblot to verify bait and prey fusion protein expression in yeast used for the SUS. The preys were revealed using anti-HA antibody and the bait (*Zm*PIP2;5) was revealed using an anti-VP16 antibody. NubG and NubWT do not contain HA-tag. The expected molecular weight of the proteins are: NubG-*Zm*VAP27-1, 40 kDa; NubG-*Zm*VAP27-2, 60 kDa, and *Zm*PIP2;5-Cub-PLV, 77 kDa. PVDF membrane Coomassie R250 staining (bottom) was used to control the protein loading. (c) Bimolecular fluorescence complementation (BiFC) signals for the pairs YFPn-*Zm*PIP2;5/YFPc-*Np*PMA2 (negative control), YFPn-*Zm*PIP2;5/YFPc-*Zm*SYP121 (positive control), YFPn-*Zm*PIP2;5/YFPc-*Zm*VAP27-1, YFPn-*Zm*PIP2;5/YFPc-*Zm*VAP27-2. BiFC signal (YFP) is shown in green, and the RFP signal in red serves as a transfection control. Scale bars, 10 µm. YFP signal was detected with a bright dot pattern for the YFPn-*Zm*PIP2;5/YFPc-*Zm*VAP27-1 and YFPn-*Zm*PIP2;5/YFPc-*Zm*VAP27-2 pairs (insets).

Figure 3. *Zm*VAP27-1 MSD is required for the interaction with *Zm*PIP2;5. (a) Domain composition of the VAP27 proteins that interact with *Zm*PIP2;5. MSD, major sperm domain; CCD, the coiled-coil domain; TMD, transmembrane domain. (b) Fluorescence ratiometric quantification from bimolecular fluorescence complementation (BiFC) experiments with the pairs PIP/PMA (YFPn-*Zm*PIP2;5/YFPc-*Np*PMA2), PIP/VAP (YFPn-*Zm*PIP2;5/YFPc-*Zm*VAP27-1), PIP/ΔMSD (YFPn-*Zm*PIP2;5/YFPc-*Zm*VAP27-1ΔMSD), PIP/ΔTMD (YFPn-*Zm*PIP2;5/YFPc-*Zm*VAP27-1ΔTMD), PIP/ΔCCD (YFPn-*Zm*PIP2;5/YFPc-*Zm*VAP27-1ΔCCD), and PIPΔC/VAP (YFPn-*Zm*PIP2;5ΔC/YFPc-*Zm*VAP27-1). For each scatter plot, the lines indicate the mean + SE. The Kruskal-Wallis and Dunn's multiple comparison test were used to calculate the statistical difference between the negative control and the remaining constructs (***, $P < 0.001$; * $P < 0.05$; ns, not significant). This experiment was repeated twice.

Figure. 4. *Zm*VAP27-1 and *Zm*VAP27-2 are in ER in close proximity to PM-localized *Zm*PIP2;5. (a, b) Confocal images (Z-stack projection) of tobacco leaf cells transiently overexpressing mVenus-*Zm*PIP2;5 and mTRQ2-*Zm*VAP27-1 (a) or mVenus-*Zm*PIP2;5 and mTRQ2-*Zm*VAP27-2 (b). Scale bars, 10 μm. (c) Inset in two confocal planes of cells overexpressing mVenus-*Zm*PIP2;5 and mTRQ2-*Zm*VAP27-1. Insets in the transmitted light panels represent in red the scanned plane (1.02 μm thin) position in the Z-stack. Arrows point to VAP27 dots. (d, e) Confocal images of cells overexpressing mVenus-*Zm*PIP2;5 and mTRQ2-*Zm*VAP27-1 after treatment with NaCl (4%) for 15 min. (d) arrows point to Hetchian strands, asterisks indicate the periplasmic space, and P is the receding protoplast. Arrows in (e) point to mVenus-*Zm*PIP2;5 vesicles surrounded by mTRQ2 signal. (f and g) Insets and fluorescence intensity profiles (arbitrary units) for mVenus and mTRQ2 in the structures pointed with the yellow arrows in (d and e): an Hetchian strand (f), and endocytic vesicle (g). Scale bars, 5 μm.

Figure 5. *Zm*VAP27-1 colocalizes with *Zm*PIP2;5 in NaCl-stress related structures. (a) Airyscan confocal images of cells overexpressing mVenus-*Zm*PIP2;5 and mTRQ2-*Zm*VAP27-1. Scale bars, 5 μm. Inset scale bars, 1 μm. (b) Airyscan confocal images of the same cell as in (a), but a different Z-position. Scale bars, 1 μm. (c-e) Airyscan confocal images of cells overexpressing mVenus-*Zm*PIP2;5 and mTRQ2-*Zm*VAP27-1 after treatment with NaCl (4%) for 15 min. (c) P, the receding protoplast, asterisks indicate to the periplasmic space. Arrows point to NaCl-induced: Hetchian strands (c), endocytic vesicles (d), and globular structure (e). (f-h) Insets and fluorescence intensity profiles (arbitrary units) for mVenus and mTRQ2 in the structures pointed with the yellow arrows in (c-e): an Hetchian strand (f), endocytic vesicles (g), and globular structure (h). Scale bars, 5 μm.

Figure 6. *Zm*VAP27-1 increases *Xenopus* oocyte P_f when coexpressed with *Zm*PIP2;5. (a) Water permeability coefficient (P_f) of non-injected oocytes (NI, control) or injected with *ZmVAP27:1* cRNA alone (7.5 ng), *ZmPIP2;5* cRNA alone (0.75 ng), or coinjected with both cRNAs in different mass ratios (1:1 or 1:10). For each scatter plot the lines indicate the mean + SE. ANOVA and Bonferroni's multiple comparison test were used to calculate the statistical difference between treatments (***, $P < 0.001$; **, $P < 0.01$; ns, not significant). The differences reported here were observed with three independent oocyte batches. (b) Relative P_f after cytosolic acidification tested in oocytes injected with *ZmPIP2;5* cRNA alone (0.75 ng), or with *ZmPIP2;5* (0.75 ng) and *ZmVAP27:1* (7.5 ng) cRNAs (1:10 ratio). The data points are representative values

obtained from the same oocyte batch (mean relative P_f + SE). This is one representative experiment of two independent experiments.

Figure 7. VAP27 protein phylogenetic analysis and conservation of the PIP-VAP27 interaction in Arabidopsis. (a) *Zm*VAP27-1 and *Zm*VAP27-2 homology group phylogenetic tree reconstructed by maximum likelihood. Branch support was assessed by the ultrafast bootstrap approximation with 1000 replicates (values ≥ 95 are represented by a blue circle). Maize VAP27-1, VAP27-2, and Arabidopsis VAP27s are shown in the tree. Branches are colored according to the taxonomy in the accompanying legends. The shadows emphasize the expansion of two different clades. (b) *At*PIP2;7 interacts with the Arabidopsis and maize VAP27-1 proteins. Bimolecular fluorescence complementation (BiFC) signals for the pairs YFPn-*Zm*PIP2;5/YFPc-*Np*PMA2 (negative control), YFPn-*At*PIP2;7/YFPc-*Zm*VAP27-1, and YFPn-*AtP*IP2;7/YFPc-*At*VAP27-1. BiFC signal (YFP) is in green, and RFP signal is in red and serves as a transfection control. Scale bars, 10 μm.

Supporting Information

Fig. S1 *Zm*VAP27-1 does not interact with *Np*PMA2, a H^+-ATPase PM resident.

Fig. S2 MSD of VAPs is required for the interaction with *Zm*PIP2;5.

Fig. S3 *Zm*VAP27-1 colocalizes with *Zm*PIP2;5 in Hetchian strands.

Fig. S4 *Zm*VAP27-1 colocalizes with *Zm*PIP2;5 in NaCl-stress related structures.

Fig. S5 *Zm*VAP27-1 increases *Xenopus* oocyte P_f when coexpressed with *Zm*PIP2;5.

Fig. S6 VAP27s in the maize genome.

Fig. S7 VAP27 protein family phylogenetic tree reconstructed by maximum likelihood.

Fig. S8 *Zm*PIP2;5 mobility in the PM is restricted in comparison with *Zm*LTi6A.

Table S1 Primers used in this work.

Table S2 Mass spectrometry peptides information.

Table S3 Potential *Zm*PIP2;5 interacting proteins.

Table S4 Proteins associated with the cytoskeleton that were pulled-down by different PIP2s.

Methods S1 . Mass spectrometry analysis

Methods S2 . Fluorescence recovery after photobleaching assay.

Table 1. Potential *Zm*PIP2;5 interacting proteins.

Identifier	Description	*P*-like value	eBayes adj. P-value	Peptide count	Unique peptides	FC
Plasma membrane proteins						
Zm00001d017526	Aquaporin PIP1-2	1.6E-06	1.01E-04	9	2	8.3
Zm00001d017526	Aquaporin PIP1-3/PIP1-4	0.0E+00	2.61E-05	10	3	17.2
Zm00001d019565	Aquaporin PIP2-6	4.2E-10	1.48E-04	7	3	7.4
Zm00001d008178	ABC transporter B family member 21	5.2E-08	2.01E-03	29	7	2.1
Zm00001d013254	ABC transporter B family member 27	8.7E-09	2.36E-04	9	3	3.3
Zm00001d043766	ABC transporter B family member 9	1.8E-08	1.80E-03	5	2	2.2
Zm00001d048823	Monosaccharide-sensing	6.9E-03	8.27E-05	2	2	26.2

	protein 2					
Zm00001d029762	Hexose transporter	1.5E-03	1.74E-02	4	3	1.6
Zm00001d005451	**Cellulose synthase A5**	3.3E-02	2.00E-02	10	3	1.7
Proteins involved in trafficking						
Zm00001d047468	**Aberrant pollen transmission1**	0.0E+00	1.18E-05	23	7	21.1
Zm00001d037842	B-cell receptor-associated 31-like	1.4E-04	4.70E-03	7	6	2.4
Zm00001d025817	**CLIP-associated protein (CLASP)**	8.6E-05	2.65E-03	12	4	2.1
Zm00001d014526	EH domain-containing protein 1	5.0E-07	1.95E-03	26	2	2.4
Zm00001d015102	Golgi SNAP receptor complex member 1	4.3E-03	2.27E-02	5	2	5.2
Zm00001d035041	Phospholipase SGR2	5.1E-03	4.82E-03	4	2	3.0
Zm00001d014159	**Protein Networked 1A**	2.0E-03	2.45E-03	5	2	2.3
Zm00001d014616	Transducin family protein / WD-40 repeat family protein	0.0E+00	2.86E-06	2	2	46.2
Zm00001d042180	**Vesicle-associated protein 27-2**	1.4E-10	8.21E-03	4	2	6.5
Zm00001d025939	**Vesicle-associated protein 27-1**	2.6E-02	2.65E-03	3	3	2.3
Zm00001d038808	Vesicle-fusing ATPase	8.7E-09	2.80E-03	35	3	2.2
Zm00001d041443	**Protein Networked 1A**	8.3E-04	6.60E-03	10	2	1.8

Zm00001d021551	Ras-related protein RABH1b	2.3E-04	1.68E-02	16	7	1.7

Proteins in bold are involved in plasma membrane (PM)-cytoskeleton organization (Pietra et al. 2013, Paredez et al. 2006, Deeks et al. 2012, Wang et al. 2014, Kirik et al. 2007).

P-like value, transformation of the probability of positive log ratio (PPLR) into a *P*-like significance score; eBayes, empirical Bayes moderated *t*-statistic; FC, fold change.

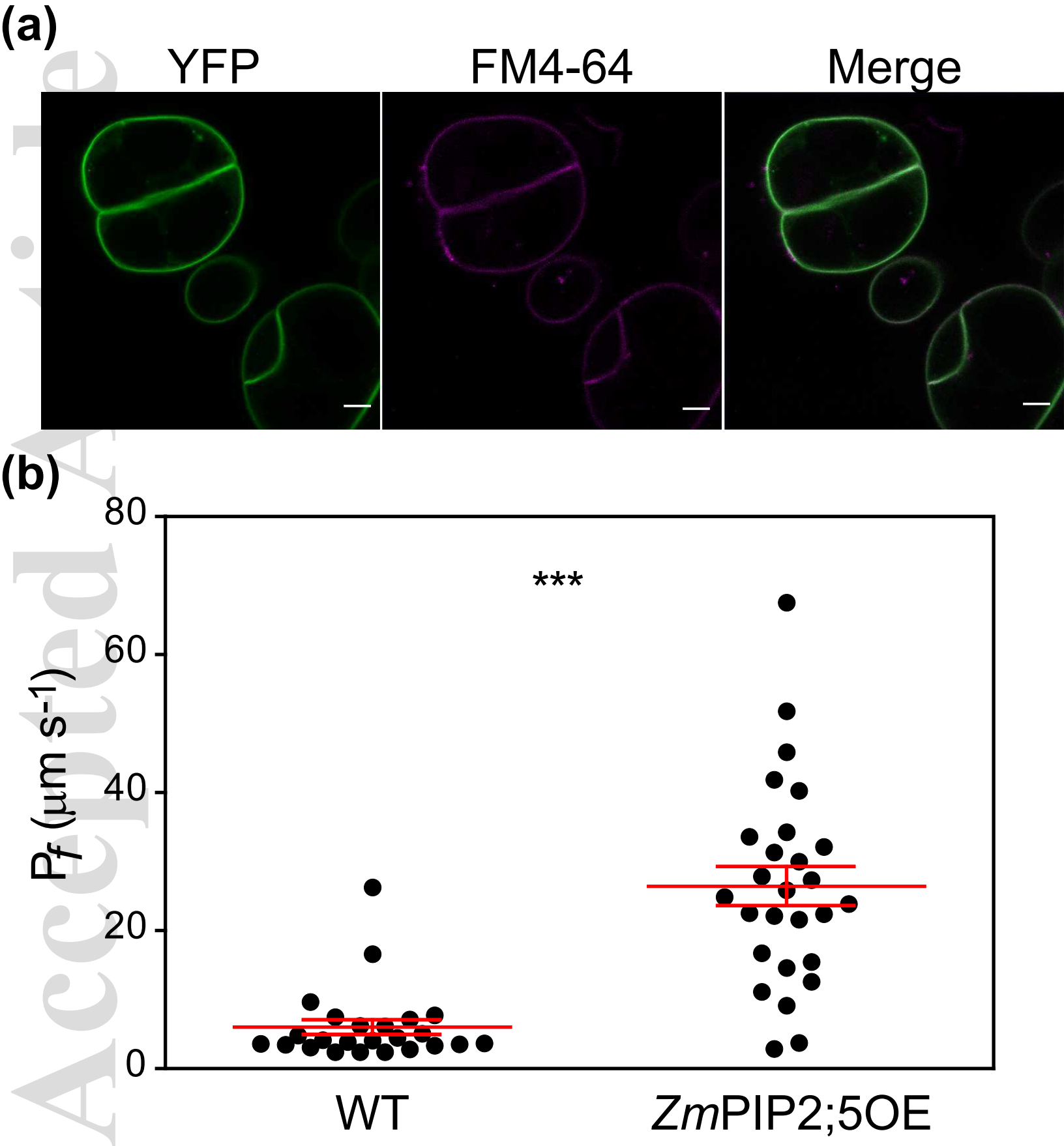

nph_16743_f1.eps

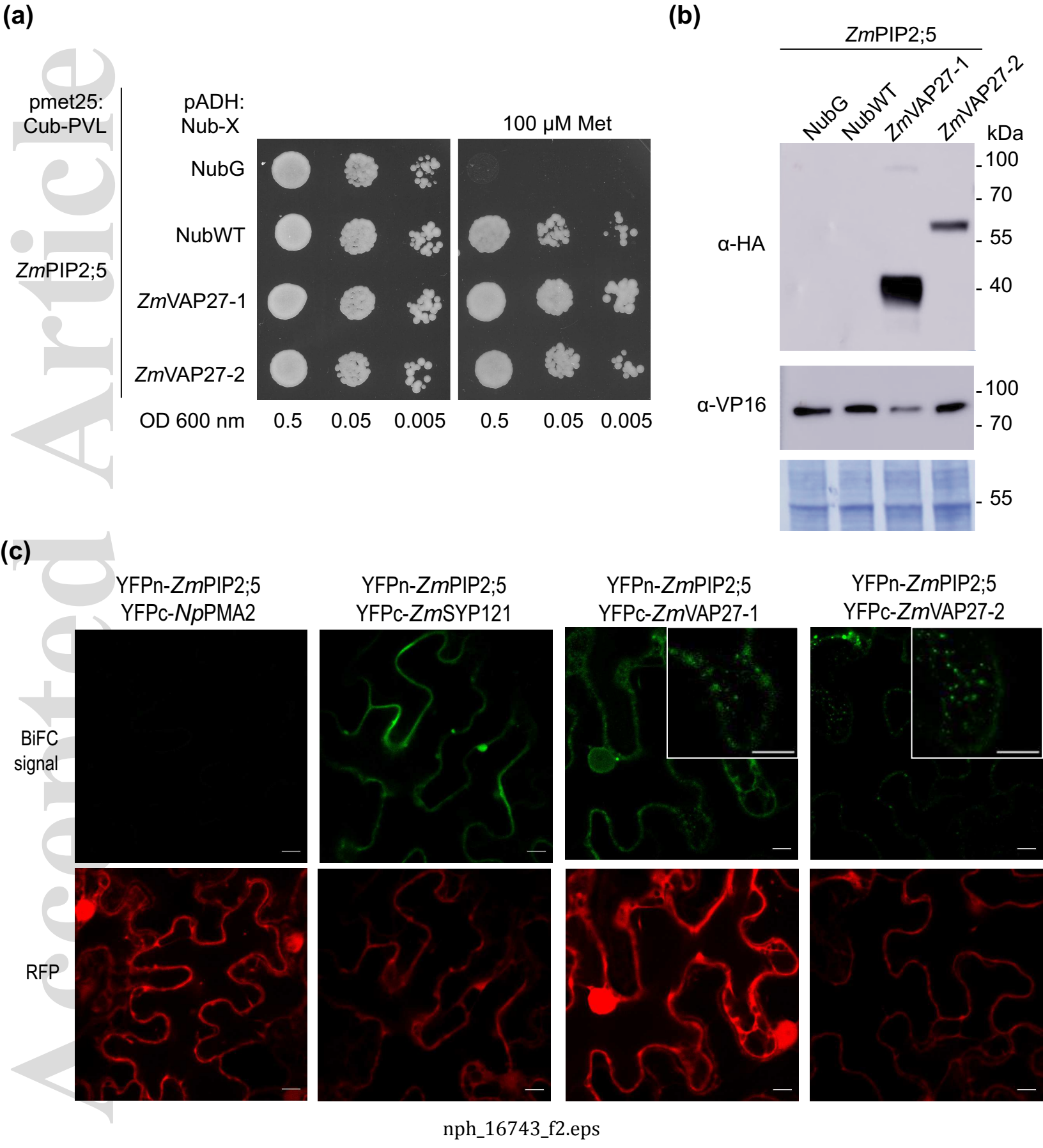

nph_16743_f2.eps

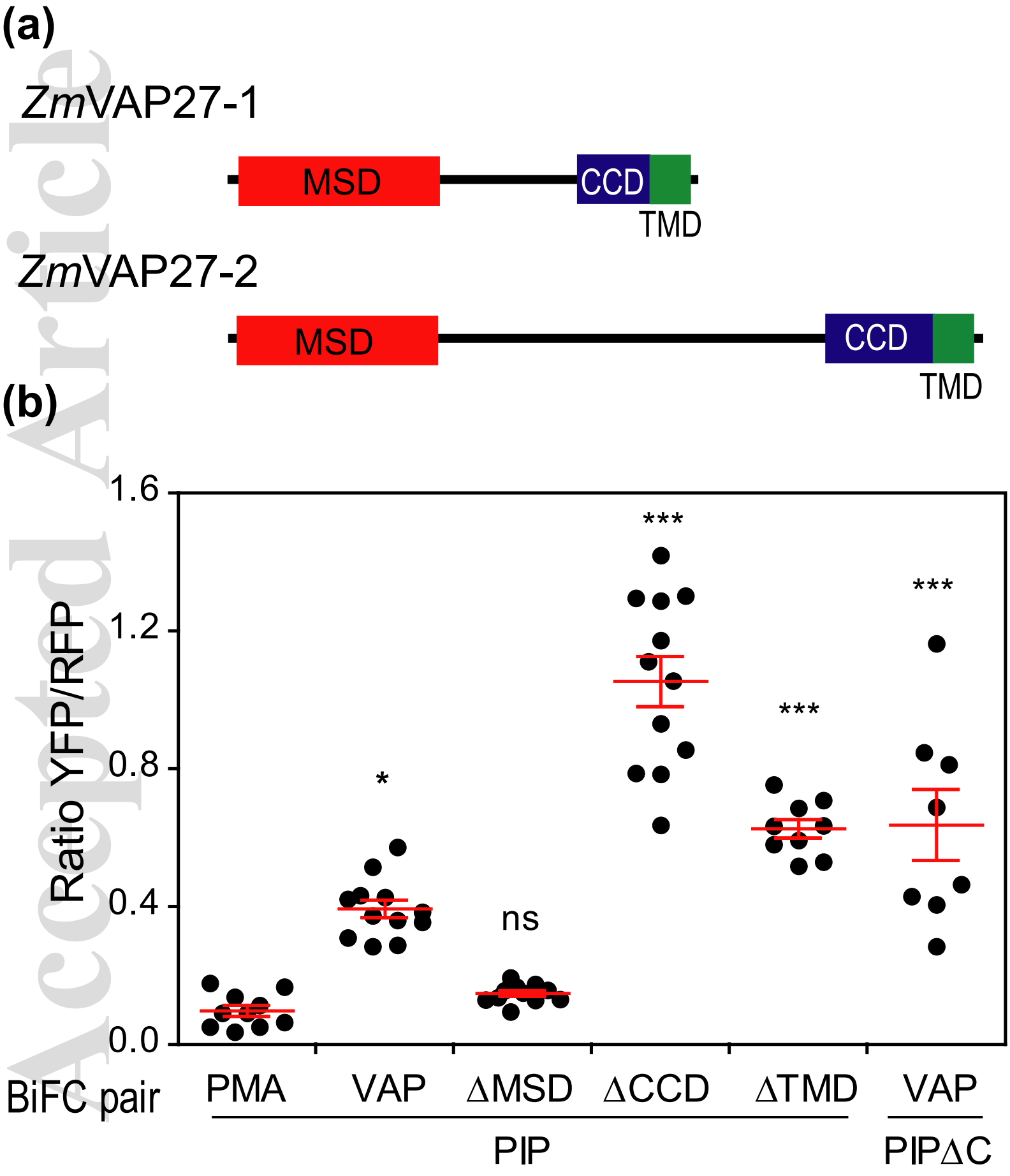

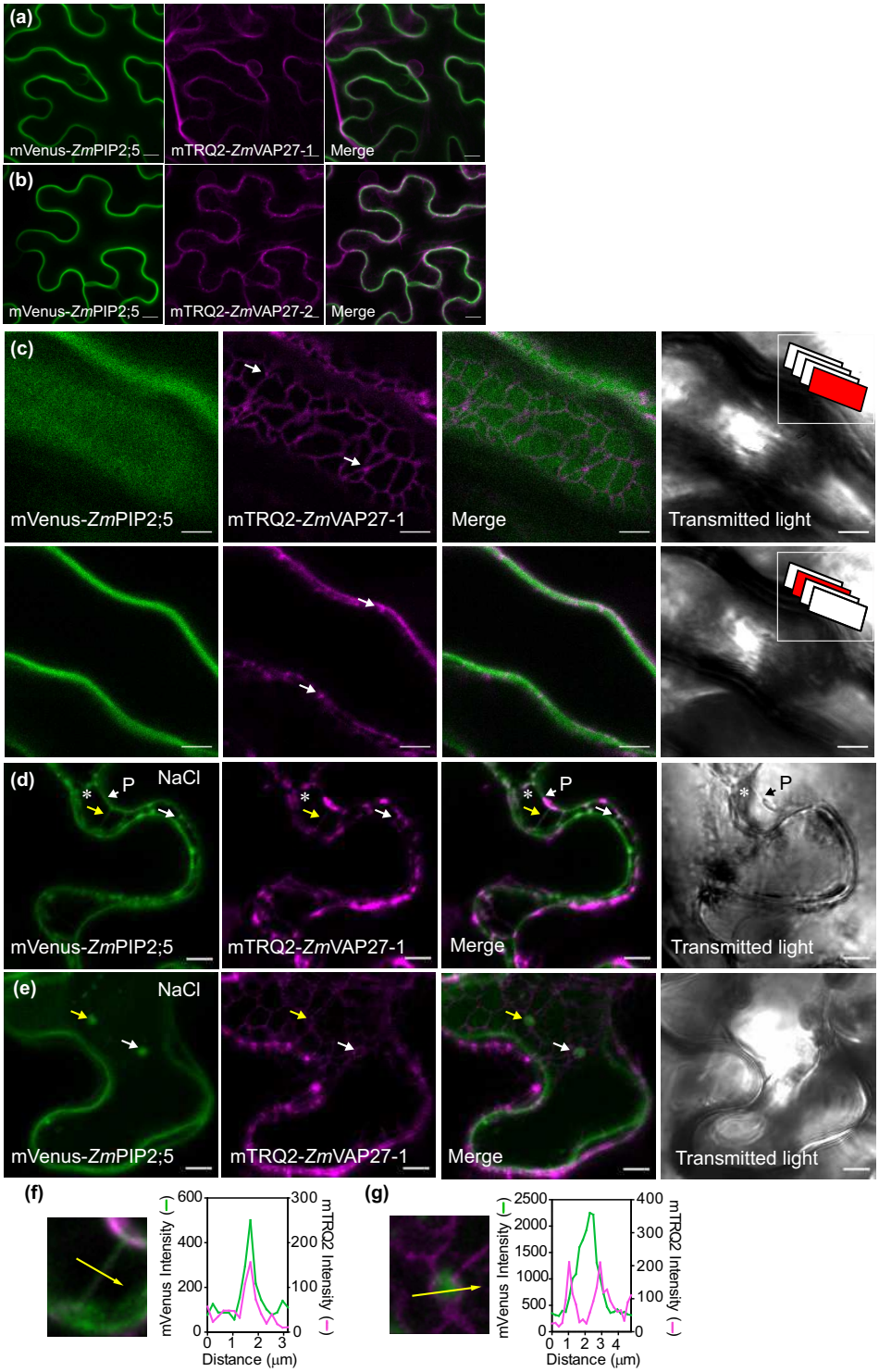

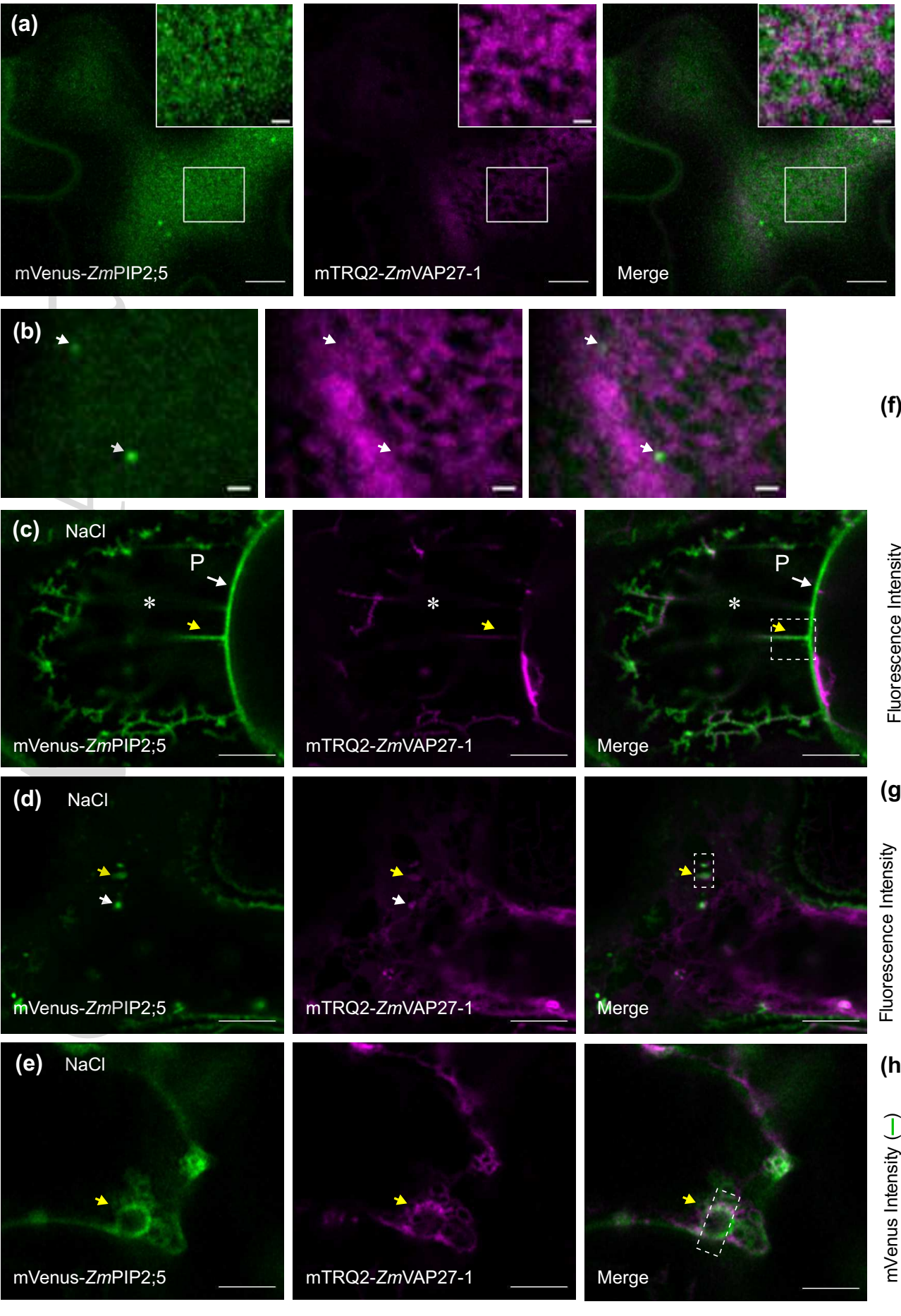

nph_16743_f5.eps

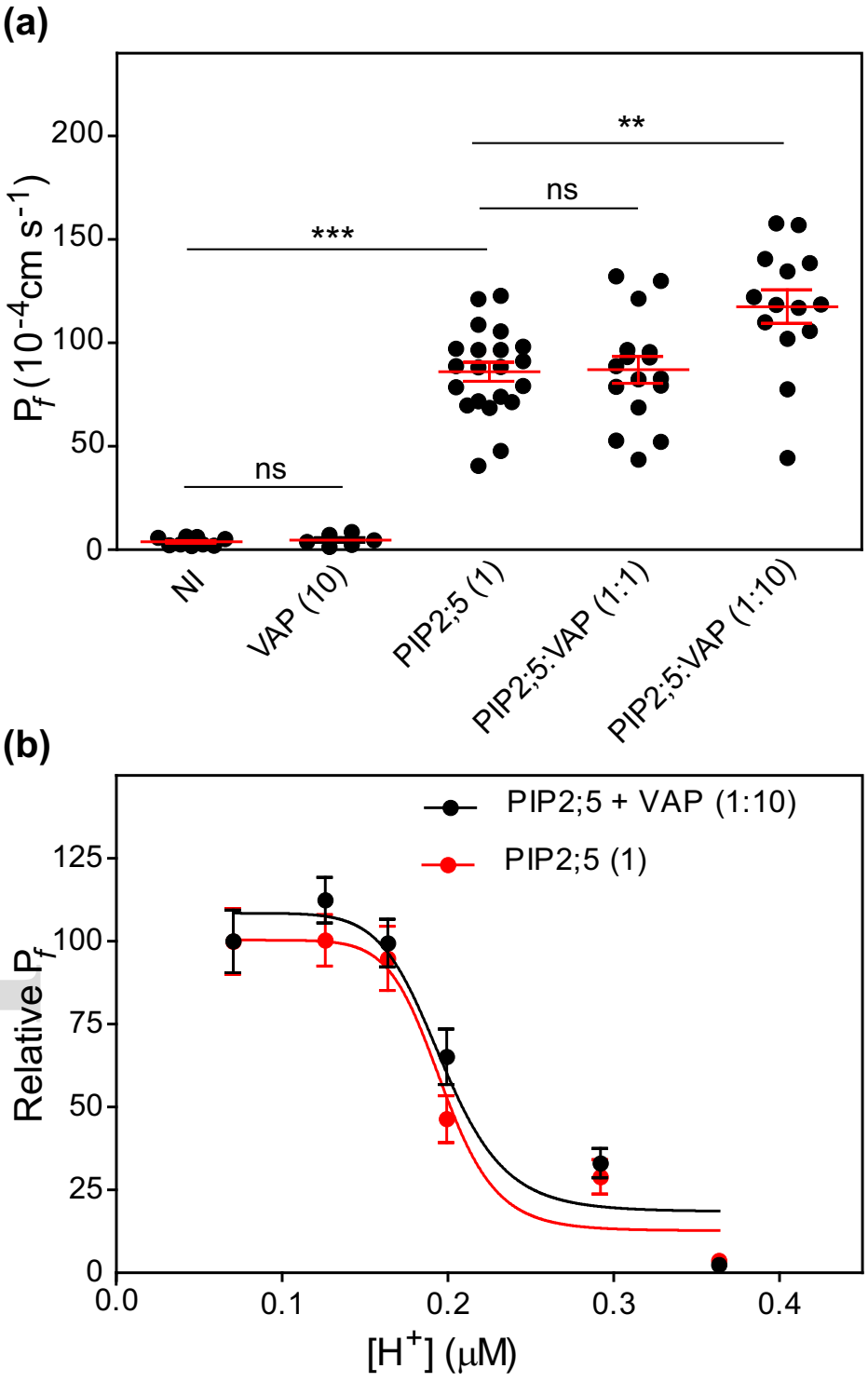

(a)

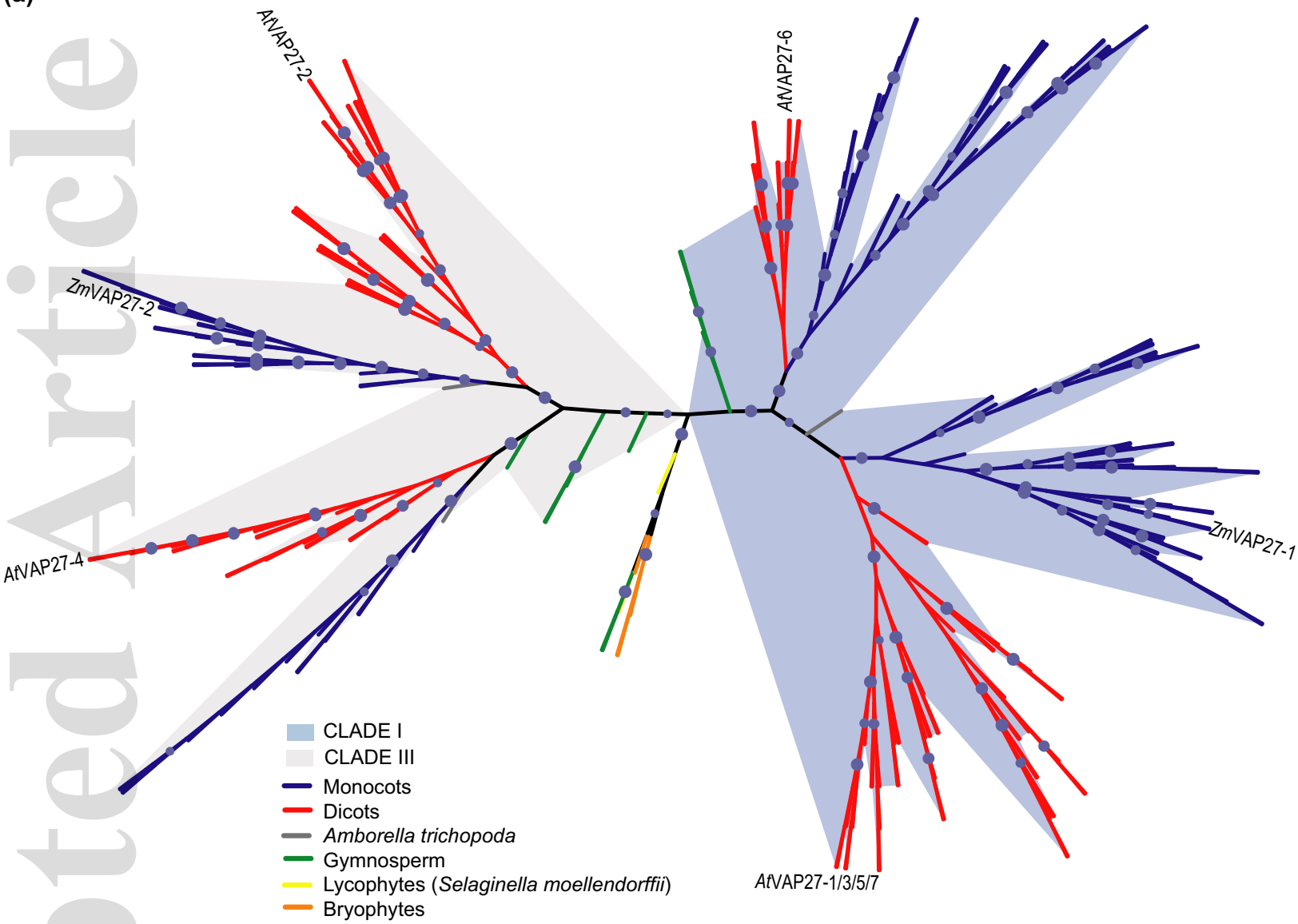

(b)

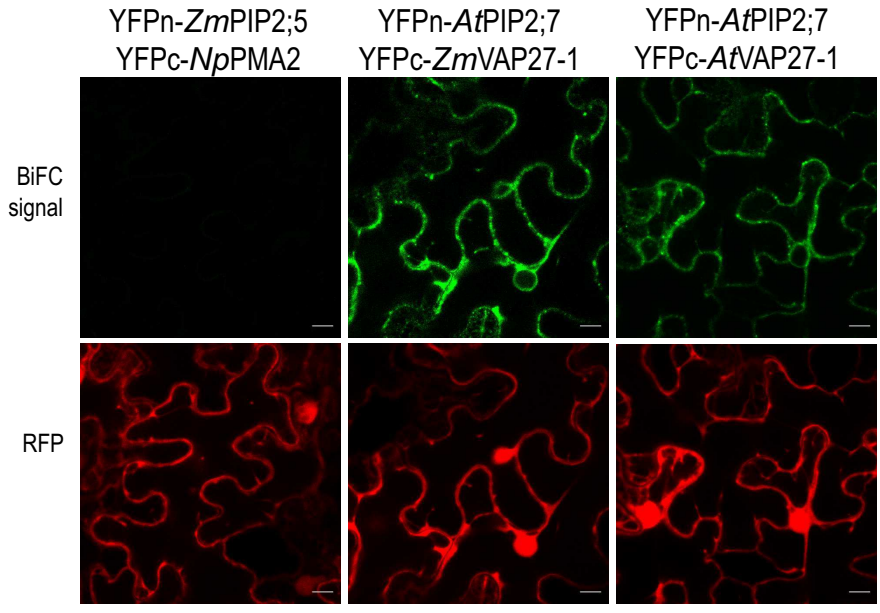

nph_16743_f7.eps